Detailed response to the editor on manuscript tc-2015-226

"Similitude of ice-sheet dynamics against scaling of geometry and physical parameters"

by J. Feldmann and A. Levermann

Dear Dr Pattyn,

We would like to thank you for handling the review process and the reviewers for their detailed look at our manuscript. We are happy with the first reviewer's assessment that our analysis is very fundamental in nature, that has been carried out for other field theories and will become very helpful in future glaciological applications. We would like to thank the reviewer for this very constructive and very positive response. Two figures have been added to the manuscript (Figs. C1 and 2), following the suggestion of reviewer #1.

Unfortunately we detected a misunderstanding by reviewer #2 of our study. We have elaborated on the purpose of our analysis in the detailed response and hope that the editor agrees with us that the analysis is not as useless as reviewer #2 is convinced it is. It would be great if our explanations below would convince reviewer #2 that we provide a useful theoretical analysis without being able to claim comprehensiveness.

Please find below the *reviewers' comments in italics* and our detailed response in blue. We have further attached a revised manuscript that highlights the changes in the submission, as well as a clean revised version.

Best wishes,
J. Feldmann and A. Levermann

Reviewer #1:

The Cryosphere - TC2015-226 *"Similitude of ice-sheet dynamics against scaling of geometry and physical parameters" by Feldmann and Levermann.*

This paper presents a similitude analysis of the Shallow Shelf Approximation (SSA) prognostic equations. Such similitude analysis which seems commonly employed in other fields or research might have been ignored by glaciologist. This contribution is therefore interesting to see the potential of such method. In this paper, the method is validated against 2D and 3D numerical simulations. Greater impacts of the paper should certainly been expected by directly applying the method to real outlets glaciers of Antarctica or Greenland, but is certainly beyond the scope of this

first paper and would certainly require further developments. This is overall a well written paper, even if it contains quite a lot of equations (which I was not able to verify all) and I would recommend its publication in TC. I have few remarks that are listed below.
Response: We would like to thank the reviewer for the readiness to review our manuscript. The reviewer comments were very constructive and helpful in improving our manuscript.

Abstract: the abstract is too long and should be shorten. There are repetitions from the abstract and introduction that could be avoided.
Response: We shortened the abstract to avoid repetitions in abstract and introduction.

page 1, line 30: I haven't done this bibliography, but people working on flubber experiment as an analogue of ice must have had these questioning about the similitude of their experiment and a real glacier. By the way, similitude of analogue experiments is an other domain of application for the method that should be mentioned.
Response: This was a very useful hint. We now mention the application of similitude analysis in laboratory glacier experiments in the abstract (page 1, lines 25-26) and in the introduction (page 1, lines 49-54) of our manuscript.

page 1, line 40 and below: I guess there are much more references than the one cited so I would suggest to use "e.g." in front of the references.
Response: We agree and added "e.g." here and in front of the next references.

page 1, line 63: I don't get the point. Which has been shown to what?
Response: We are sorry for the lack of clarity and have tried to make this clearer (page 2, lines 11-14).

page 2, line 14: I don't understand what you mean by "which will be put to test in the forthcoming MISMIP+ intercomparison project"?
Response: This phrase is indeed out-of-context and thus we deleted it.

below Eq. (1): not all the notations introduced in this equation are explained (e.g. A).
Response: Thanks for the hint. We indeed missed to introduce ice density ρ and gravitational acceleration g and added them below Eq. (1) (page 2, lines 92-93). Ice softness A was already introduced in the line above Eq. (1).

Equation (4) is neglecting basal mass balance (basal melting). It should be mentioned.
Response: That's true. We added a sentence below Eq. (4) (page 3, lines 20-23).

page 3, line 20: the use of compression is confusing as compression could refer to the state of stress. Elongation/Shortening?
Response: We are glad for the reviewer's suggestion and replaced the terms here and elsewhere in

the manuscript.

page 3, lines 49-51: I am not sure to clearly understand the two limits. Especially the case $\Phi >> \theta$ since the case of a frozen bed cannot be modeled assuming the SSA. Also, to which equations do you refer when you said "in which non of the stress balance terms are neglected"? In the SSA, this is already not true as it neglects stress regarding to the Stokes equations. This should be clarified.

Response: These lines were indeed misleading (especially the statement about the $\Phi >> \theta$ limit is incorrect, as noted by the reviewer). We re-formulated the paragraph accordingly (page 3, lines 54-59).

page 4, line 30: it is not the length of the entire ice-sheet, but only the grounded part (upstream the GL).

Response: We thank the reviewer for the hint and corrected the line.

page 4, line 29: integration of (Eq. 4) over -> integration of Eq. (4) over (and at other places in the manuscript)

Response: Done. At other places "(Eq. x)" is intended to avoid double brackets, i.e. (Eq. (x)), see, e.g. page 4, line 81. If applicable, we will be glad to change the notation according to the TC conventions in the final typesetting phase.

page 4, lines 31-35: I am not sure to follow what is really demonstrated here and not sure to see where is the consistency with the BLT of Schoof. Indeed, the equations derived by the BLT are based on the SSA ones, so that intuitively I would said that the similitude derived for the SSA also apply for the BLT? You should present it the other way, and derive directly the scaling relation (24)?

Response: This remark was indeed second by the second reviewer and we really appreciate that the reviewers demand that we reconsider this section. Please consider the following: The Shallow Shelf Approximation is a non-linear differential equation and the solution by Christian Schoof required a few additional assumptions, for example he omitted the membrane stresses in the stress balance and reintroduced them in the boundary conditions. He also does not consider a time dependence which we reintroduce in the commonly used way via the mass continuity equation. Given these differences we think it is not completely trivial that the SSA-scaling that we derive survives all the way to the final solution given by Schoof (2007b). Obviously it has and that makes it almost look trivial again. In any case we tend to think that it is at least a nice illustration of the scaling in one of the solutions of the SSA equation which is a simpler equation than the full SSA. We would be willing to omit this section if demanded by the editor and reviewers, but we would prefer to keep it in, if possible.

page 5, line 45: Is it really constant, which refer to time, whereas here one wants to said that it is the same value of the friction in the two experiments. "Same" or "identical" is may be

better than "constant"? It should be modified accordingly all along the manuscript.
Response: We are glad for the valuable hint and changed the terms here and in the rest of the manuscript.

page 5, line 48: reference to Table 2 is broken
Response: Done.

page 5, line 53: it should be mentioned here that the bedrock also varies in the transverse direction.
Response: Done.

page 6, line 26: Vialov profiles are derived assuming the Shallow Ice Approximation (SIA) whereas here the SSA is used. Only in the conclusion it is mentioned that in a previous paper you have shown that SSA was conducting to similar profils as Vialov ones. It should be mentioned here.
Response: Done.

page 6, line 71: atmosphere: Rising -> atmosphere: rising (and at other places in the manuscript)
Response: Done.

page 6, line 82: space (Fig. 7 accounts for only one value of m. -> space (Fig. 7 accounts for only one value of m).
Response: Done.

page 7, line 22: To what refers "respectively"?
Response: Corrected.

page 7, line 33: I don't understand what you mean here as you have already started from the SSA equations and not the full Stokes system of equations. There is a missing citation.
page 7, line 40: again, is used to derive the SSA from the Stokes equations so it has somehow been used already in the equations you are using here. This part is a bit confusing and would require some clarifications
Response: We thank the reviewer for the careful reading. We re-worded the paragraph (page 7, lines 60-71) to be more precise about what we want to say and in particular make clear that we consider the **SSA** stress balance here (previously we somewhat sloppily only wrote stress balance).

page 7, line 50: As already mentioned, I would said, but may be I misunderstood something, that this is normal as these BLT equations are derived from the SSA ones...
Response: Please see our response to the above comment related to page 4 lines 31-35.

page 7, line 103: law still then still depends on -> law then still depends on
Response: Done.

page 7, line 106: of m (9): Vertical -> of m (9): vertical
Response: Done.

page 8, line 18: reasonably - and this should be said before.
Response: Done. Also see above.

page 8, lines 37-38: consider rewording and also avoid the repetition for the value of n.
Response: Done.

page 10, line 33: to Eq. 27 with -> to Eq. (27) with
Response: Done.

B1: define what is RHS and LHS
Response: Done.

page 11, line 28: instantaneously, elimination
Response: Done.

Figures 5 and 6: legend and axis label are not correct.
Response: These must have got broken during the TCD publishing phase since the original submitted file had correct labels and legends as is the case for the revised manuscript.

Why not applying a scaling along x and t? How do you choose the part of the curve where is made the retreat rate comparison?
Response: We thank the reviewer for the useful hint to scale the time series along both axis. In the scaled plots the curves of grounding-line position during the ice-sheet instability collapse approximately into a single curve, indicating similitude between the experiments as expected from theory (Figs. C1 and C2). At the same time it is most important to us to visualize the variety of retreat rates (slopes) during unstable grounding-line retreat simulated in our scaling experiments (Figs. 5 and 6). We thus are in favor of keeping the original unscaled plots in the results section and included the scaled plots into the Appendix (Appendix C).
The range, i.e. the section of the curve, for the retreat-rate comparison (visualized in Figs. 5 and 6) was chosen by hand originally. We now use an objective criterion to define that range (x-range +- 50 km around the minimum of the bed depression) within which we fit the slopes of approximately constant grounding-line retreat. We updated Figs. 5 and 6 and their captions accordingly.

In the legend: overlayn -> overlaid
Response: Done.

legend Fig. 7: to Eq. 32. -> to Eq. (32).
Response: Done.

legend Fig. 9: to Eq. 31 for -> to Eq. (31) for
Response: Done.

Reviewer #2:

Review of a manuscript "Similitude of ice-sheet dynamics against scaling of geometry and physical parameters " by J. Feldmann and A. Levermann.

The manuscript presents similarity solutions for the isothermal Shallow Shelf Approximation (SSA) equations. Though, to my knowledge, such solutions for the SSA have not been derived before, the manuscript has a number of conceptual inconsistencies and cannot be published in its present form.

Response: This criticism is in stark contrast to the assessment of the first reviewer and as we will show below the criticism is not substantiated by the reviewer. The requests made by the reviewer are by large extensions of our work. We, however, agree with the first reviewer that our manuscript is indeed already quite long and has a proper scope. We would like to emphasize that we do not attempt to give a comprehensive analysis of glaciers, but simply apply a very fundamental method to one of the two most commonly used approximations of the primitive equations of ice dynamics. We agree with the first reviewer that this analysis will turn out to be helpful in a number of future applications. Our analysis is based on a number of assumptions that are clearly and transparently emphasized in the manuscript. For example we assume an isothermal glacier. This is an obvious reduction of generality of our analysis, but it does not render it useless. In fact reduction in generality always occurs when an approximation is applied. As an example, the Shallow Ice Approximation is only rigorously valid when the ice is frozen to the ground which is not necessarily true in ice streams, but despite this constrain on the applicability of the approximation, it turned out to be very useful in glaciological theory. While we appreciate the comments made by the reviewer and have used them to improve our manuscript where this was possible, we would appreciate if we could keep the core of our analysis as it is.

Major concerns

The first major concern is an assumption that ice is isothermal and the independence of the ice softness parameter of other parameters, e.g. ice thickness or surface mass-balance. Thicker ice is usually softer than thinner ice, hence more deformable. Physically, $A^{-1/n}$ decreases with increasing ice thickness. The constant ϑ (eqn. 9) implies the opposite. Though, mathematically there is nothing wrong with this assumption, the derived similarity solutions are not suitable for glaciological applications. One possibility to resolve this inconsistency could be to consider temperature itself (or depth-averaged or depth-integrated temperature) instead of the ice softness parameter A. It still can be spatially uniform in the horizontal direction, but vary with an ice-stream of ice-shelf characteristic thickness.

Response: We appreciate the reviewer's concern. Perhaps we have not made it clear enough that the theory that we derive is only valid under certain assumptions. The assumption of isothermal

ice was mentioned in the abstract and a number of times in the manuscript itself. There is a vast amount of glaciological theory published that assumes isothermal ice (see added references on page 2, lines 7-9). It is a strong assumption which is not always valid but it allows for insights into other aspects of ice dynamics that do not depend strongly on the spatial and temporal thermal structure of the ice. Obviously the temperature dependence of the softness is accounted for in these kind of theories, but the changes with space and time are neglected. We have now changed the introduction (page 2, lines 4-9) as well as the discussion (page 8, lines 90-103) to make it clearer that we assume isothermal ice and that our conclusions are only valid within this restriction. Future analysis not assuming isothermal ice but allowing for a spatial distribution of temperature within the ice might be interesting even though in that case it would have to be decided which is a generic spatial structure that can be assumed without restricting the results too strongly. In order to get results that fully integrate the thermal evolution of the ice sheet, numerical models are of course available.
At this stage, we would appreciate if the editor and reviewer would allow us to keep the analysis restricted to isothermal ice after we have now further emphasized that this is a restriction..

The second major concern is the chosen dependence of the surface mass-balance ratio δ on the friction-coefficient ratio γ (eqn. 15). Physically, the surface mass-balance depends on a climate, and has no connection to ice-stream properties like basal friction. Though, there is a connection between the basal friction coefficient and the ice stiffness parameter (eqn. 16), it is very weak, as frictional heating affects ice temperature, hence its stiffness, only very small part of the ice column, close to its bottom.
Response: This comment by the reviewer leads us to suspect that the reviewer has not fully understood the idea of scaling analysis in general and our analysis in particular. We do, of course, never assume that the surface mass balance ratio depends on the friction coefficient. We would have no grounds for that. The equation that the reviewer is referring to is a **result** as opposed to an assumption. Perhaps it helps to paraphrase the spirit of these kind of scaling analysis as follows: **If** two ice sheets are self-similar **then** these relations have to be fulfilled. That is to say: if for example you find a glacier with a certain ice thickness and a certain bed slope etc. and if this glacier has the same qualitative profile as another one which however has a different thickness and a different bed slope etc. then our analysis shows (for isothermal ice) that the basal friction and the surface mass balance need to have a specific relation otherwise this glacier cannot be in equilibrium with its environment and the SSA equation. We are sorry that our manuscript obviously was not clear enough for the reviewer to understand this point and are glad that the first reviewer understood the concept. We have tried to make this now clearer in the manuscript (page 7, lines 94-104).

There is no relevance of the similarity solutions derived in this study to the Shoof's (2007) boundary layer theory. The system of equations considered in both studies is the same, so it is not surprising that the flux formulation is identical (in a non-dimensional form).
Response: Please see our response to the same remark made by reviewer #1 in reference to page 4 lines 31-35.

Throughout the text, the described ice flow is referred to as "ice-sheet" flow. This is misleading, because the SSA equations are valid only in ice-stream and ice-shelf settings, and are inapplicable to the rest of an ice sheet. Equally, the use of the Vialov profile (even as a motivation) is incorrect. This profile is derived based on the Shallow Ice Approximation (SIA).

Response: The SSA has been used to describe the dynamics of ice sheets before, for example by Schoof (2007a), Goldberg et al. (2009), Gudmundsson et al. (2012), and whenever SSA-only modes are used in model intercomparisons. While it is true that the SSA has restrictions, for example that it can only be used for the depth-averaged horizontal flow, it is not true that it is a completely invalid representation of ice sheet flow. We however appreciate the reviewers concern and have changed the phrase "ice sheet flow" to "ice flow". I think that it is clear to the reader that we only analyze SSA dynamics. We have also made some changes in order to highlight that the Vialov profile is derived from the SIA equation (page 6, lines 47-52). In the manuscript we use it for comparison with an analytic result. We believe that this is enlightening for the reader and that omitting this comparison would be a shame. Since we do nothing unscientific or intransparent here, we would appreciate if we could keep it in.

The mass-conservation equation (4), for some reasons called in this study the "ice thickness equation (ITE)", omits the basal mass-balance. This may be appropriate for ice streams, however, on ice shelves with strong basal melting neglecting this term is incorrect.

Response: We are grateful for the reviewer's scrutiny, but again this comment is not relevant to our analysis. We never said that we study ice shelves in the presence of basal melt as there are a lot of things we do not study. Equivalent equations to those we derive here are present in every textbook of hydrodynamics for about 100 years (I personally own a copy of the book by Sir Horace Lamb from the 19th century which describes the similarity analysis for the Navier-Stokes equation). To our knowledge these equations are, however, not present in the glaciological literature for the SSA dynamics. Thus, while we do not claim to be comprehensive in our analysis in the sense that we have a theory for all ice dynamics, we believe that these equations make some scientific contribution in their present form and would be grateful if we could publish them without including basal melt. In order to avoid misunderstanding, we now make clear in the text where we define the ice thickness equation (Eq. 4) that throughout the study we focus on the grounded part of the ice sheet and that we neglect the basal mass balance (page 3, lines 21-24 and lines 57-58; page 4, lines 47-48). The term "ice thickness equation" is used frequently in glaciological textbooks and we would like to keep it here.

The abstract implies that the similarity analysis has never been applied in glaciology. This is not true; Halfar (19833) and Buler et al. (2005) describe similarity solutions for various configurations of the SIA.

Response: We thank the reviewer for this helpful advice. We modified the abstract and now provide examples for previous use of the similarity concept in the field of glaciology in the introduction, including the mentioned similarity solutions for the SIA and laboratory experiments

in which glacier flow is simulated using a replacement material for ice (page 1, lines 48-58).

Minor concerns

P. 3 Line 20 $\alpha, \beta < 1$ suggests that α and β can be negative.
Response: We thank the reviewer for the hint and added 0 as the lower bound.

P.3 Lines 41-51. Sentences starting with "In Eq. (9). . . " do not make sense. A statement "$\psi >> \vartheta$, holding for ice frozen to bedrock" is incorrect. The SSA is inapplicable in circumstances where ice is frozen to bedrock.
Response: We are grateful to the reviewer for pointing to this statement that is indeed incorrect in the SSA context. We re-formulated the paragraph.

P. 3 eqn (14) and P.4 eqn (17), though mathematically are correct, physically not so. The ice softness and surface mass balance are unlikely scale identically. The basal friction is independent (to a leading order) of the surface mass-balance.
Response: Please see our answer to the reviewers second "major concern". This is not a claim we make, it is a result of the similarity assumption and thus one of the consequences for "similar ice geometries". Since ice softness and surface mass balance can vary independently it would indeed be invalid (to put it mildly) to assume that they scale with each other, but we do not do this. We hope this has become clearer in the text now.

P.5 Lines 50-55. The numerical simulations are one-dimensional (a flow-line setup) and two-dimensional (channel-flow setup). The SSA are vertically integrated equations and do not have vertical dimension.
Response: That is correct and so is our analysis. We do not see a problem here, but perhaps we are missing the reviewer's point here.

In many places references are missing (e.g. p.7 line 34).
Response: Done.

In summary, the presented similarity analysis of the SSA equations has little to do with ice-stream and ice-shelf flow. The derived set of the dimensionless parameters is perfectly fine for an abstract set of equations of the SSA form. However, shortcomings of the study described above most likely lead to erroneous conclusions of the similarity behaviour of the ice streams, ice shelves and grounding lines.
Response: We are happy that the reviewer assesses our similarity analysis to be mathematically "perfectly fine". In light of the fact that similar analysis for the Navier-Stokes equation have been used for decades to build airplanes and ships and have been proven tremendously helpful for the theoretical understanding of hydrodynamic flow, we are confident that our analysis is not completely useless. While we cannot hope to have similar impact on the glaciological community

as the hydrodynamics similarity analysis, we believe that this analysis is at least useful enough to be published.

Similitude of ice-sheet dynamics against scaling of geometry and physical parameters

J. Feldmann[1,2] **and A. Levermann**[1,2,3]

[1]Potsdam Institute for Climate Impact Research (PIK), Potsdam, Germany
[2]Institute of Physics, University of Potsdam, Potsdam, Germany
[3]LDEO, Columbia University, New York, USA

Correspondence to: A. Levermann (anders.levermann@pik-potsdam.de)

Abstract. The concept of similitude is commonly employed in the fields of fluid dynamics and engineering ~~where scaling laws are derived from the governing equation of flow dynamics, e.g., the Navier-Stokes equation. Here we transfer~~ but rarely used in cryospheric research. Here we apply this method to the problem of ~~ice-sheet~~ ice flow to examine the dynamic similitude of ~~ice sheets~~ isothermal ice sheets in shallow-shelf approximation against the scaling of their geometry and physical parameters. Carrying out a dimensional analysis of the stress balance ~~for isothermal ice sheets in shallow-shelf approximation~~ we obtain dimensionless numbers that characterize the flow~~, similar to the Reynolds or Froude numbers in fluid dynamics~~. Requiring that these numbers remain ~~constant~~ the same under scaling we obtain conditions that relate the geometric scaling factors, the parameters for the ice softness, surface mass balance and basal friction as well as the ice-sheet intrinsic response time to each other. We demonstrate that these scaling laws are the same for both the (two-dimensional) flow-line case and the three-dimensional case and that they are consistent with flow-line boundary-layer theory. The theoretically predicted ice-sheet scaling behavior agrees with results from numerical simulations that we conduct in flow-line and three-dimensional conceptual setups. ~~In a set of experiments the setup geometry is scaled systematically and the physical parameters are prescribed according to the derived scaling laws.~~ We further investigate analytically the implications of geometric scaling of ice sheets for their response time~~under constant basal conditions finding that thicker (thinner) ice sheets have a shorter (longer) response time and that the opposite holds for the horizontal ice-sheet extent.~~. With this study we provide a framework which, under several assumptions, allows for a fundamental comparison of the ice-dynamic behavior across different scales. It proofs to be useful in the design of conceptual ~~model setups but~~ numerical model setups and could also be helpful for designing laboratory glacier experiments. The concept might also be applied to real-world systems, e.g., to examine the response times of glaciers, ice streams or ice sheets to climatic perturbations.

1 Introduction

In the fields of fluid dynamics and engineering scaling laws are used to perform experiments with spatially reduced models in water channels or wind tunnels to predict the behavior of the associated full-scale system (e.g., Scruton, 1961; Li et al., 2013). Dimensional analysis and the principle of similitude allow to derive such scaling laws analytically (e.g., Rayleigh, 1915; Macagno, 1971; Szücs, 1980). For instance, a dimensional analysis of the Navier-Stokes equation (Kundu et al., 2012) yields the Reynold's number (Reynolds, 1883) as one of the dimensionless parameters of the governing equation which characterize the dynamics of fluid flow. Under the assumption of the similitude principle the Reynold's number can provide a scaling law for the fluid's characteristic linear dimension, velocity and viscosity that assures similar flow patterns. The principle of similitude is applied well beyond the field of engineering, e.g. in zoology (land mammals move in dynamically similar fashion at equal Froude number, Alexander and Yayes, 1983) or biology (Stahl, 1962).

The similitude concept is also applied to some extent in the field of glaciology: in laboratory glacier experiments dimensionless numbers like the Reynold's, Froude and Ramberg numbers are used to check for (dynamic) similarity between the geometrically scaled model (based

on the properties of the analogue ice material) and the real-world system (Burton et al., 2012; Corti et al., 2014). In Halfar (1983) and Bueler et al. (2005) the similitude principle is used to derive similarity solutions of the shallow-ice-approximation (SIA, Hutter, 1983) of the full-Stokes stress balance for the case of an isothermal, radially symmetric ice sheet.

Here we apply the concept of similitude to ~~ice-sheet dynamics . Our investigation is~~ the dynamics of idealized ice sheets based on the shallow-shelf approximation (SSA, Morland, 1987; MacAyeal, 1989; Greve and Blatter, 2009)~~) of the full-Stokes stress balance~~. In particular we assume isothermal ice and a spatially uniform basal friction coefficient, conditions that have been used to analyze ice-sheet dynamics in a number of previous studies (e.g., Dupont and Alley, 2005; Goldberg et al., 2009; Gudmundsson et al., 2012; Pattyn et al., 2013; Asay-Davis et al., 2015). Neglecting the terms of vertical shearing in the stress balance and accounting for the small thickness-to-length ratio of ice sheets, the SSA represents the relevant dynamics of floating ice shelves and grounded ice streams~~, i. e., regions~~. The capability of numerical SSA models to simulate these regimes that are characterized by fast plug-like flow ~~, which has been shown in numerical applications~~ has been demonstrated in various studies (e.g., Goldberg et al., 2009; Gudmundsson et al., 2012). The SSA can be complemented by the ~~shallow-ice approximation~~ SIA (Huybrechts, 1990; Sato and Greve, 2012) to also include vertical shearing, which is dominant in the more stagnant interior parts of an ice sheet (Bueler and Brown, 2009; Pollard and DeConto, 2012; Thoma et al., 2015), whereas higher-order approximations (Schoof and Hindmarsh, 2010; Larour et al., 2012; Cornford et al., 2015) neglect less stress components in the full-Stokes stress balance (Favier et al., 2012). The MISMIP3d benchmark revealed that numerical models applying the SSA can capture grounding-line dynamics comparable to more elaborate models in conceptual experiments (Pattyn et al., 2013; Feldmann et al., 2014)~~which will be put to test in the forthcoming MISMIP+ intercomparison project~~.

A dimensional analysis of the ice-dynamic equations is often carried out to compare the magnitudes of the different acting forces and thus to derive physically motivated approximations, as done when deriving the SSA from the full-Stokes stress balance (MacAyeal, 1989; Greve and Blatter, 2009). The non-dimensionalized form of the SSA itself and the involved dimensionless coefficients that result from the introduction of typical scales for, e.g., ice-sheet thickness and velocity, have been used to consider asymptotic limits of SSA ~~ice-sheet~~ ice flow in previous work (Schoof, 2007a; Dupont and Alley, 2005; Tsai et al., 2015; Haseloff et al., 2015). In the present study we utilize these coefficients to derive ice-sheet scaling laws for the geometry, response time and other physical ice-sheet parameters, a step that to our knowlegde, has not been taken before. The scaling behavior of ice sheets, that here is analyzed in a conceptual way, might be of use to better understand the large-scale evolution of the polar ice sheets. Of particular interest is the scaling of the ice-sheet response time (Levermann et al., 2013, 2014) against the background of Antarctic instabilities (Weertman, 1974; Schoof, 2007b; Rignot et al., 2014; Fogwill et al., 2014; Mengel and Levermann, 2014). The time scales of possible rapid ice discharge due to instability in the past (Pollard and DeConto, 2009; Pollard et al., 2015) and future (Favier et al., 2014; Joughin et al., 2014; Feldmann and Levermann, 2015b) are highly uncertain.

The paper is structured as follows: ~~In~~ in the next section the governing equations in SSA are non-dimensionalized to derive ice-sheet scaling laws for one and two horizontal dimensions, respectively. We also give an alternative approach to derive the same scaling conditions. Afterwards the analytically predicted ice-sheet scaling behavior is compared with results from numerical modeling. To this extent conceptual experiments are designed in two and three spatial dimensions. Steady states as well as the transient response to perturbation of the simulated ice sheet are analyzed for a systematic variation of the scaling parameters which are prescribed according to the scaling laws. We then examine analytically the implications of the scaling conditions for the response times of ice sheets considering the geometric scaling factors and basal friction parameter as independent variables. Eventually we discuss the results and conclude.

2 ~~Similarity~~ Similitude of shallow ice-sheet dynamics

Here we derive scaling laws that determine how the geometry, response time and the involved physical parameters for ice softness, surface mass balance and basal friction have to relate in order to satisfy similitude between different ice sheets. This is visualized conceptually in Fig. 1 for two ice sheets which differ in vertical and horizontal scale. Based on the governing equations in dimensionless form, we obtain dimensionless scale factors which depend on the scales of the geometric and physical parameters of the ice sheet. The requirement that each of these factors has to remain ~~constant~~ the same under a scaling of the parameters makes sure that the dynamic equations remain exactly the same. The resulting scaling laws thus put constraints on the parameter scaling, ensuring similitude between the different ice-sheet configurations.

2.1 Basic equations for similitude analysis

The problem addressed here is the one of an isothermal ice-sheet in SSA (Greve and Blatter, 2009). The two horizontal components of the stress balance in SSA with spatially uni-

form ice softness A are given by

$$\begin{aligned} &A^{-1/n}\left(\frac{\partial}{\partial x}\left[H\dot{\epsilon}_e^{1/n-1}\left(2\frac{\partial v_x}{\partial x}+\frac{\partial v_y}{\partial y}\right)\right]\right.\\ &\left.+\frac{1}{2}\frac{\partial}{\partial y}\left[H\dot{\epsilon}_e^{1/n-1}\left(\frac{\partial v_x}{\partial y}+\frac{\partial v_y}{\partial x}\right)\right]\right)+\tau_{b,x}=\rho g H\frac{\partial h}{\partial x},\\ &A^{-1/n}\left(\frac{\partial}{\partial y}\left[H\dot{\epsilon}_e^{1/n-1}\left(2\frac{\partial v_y}{\partial y}+\frac{\partial v_x}{\partial x}\right)\right]\right.\\ &\left.+\frac{1}{2}\frac{\partial}{\partial x}\left[H\dot{\epsilon}_e^{1/n-1}\left(\frac{\partial v_y}{\partial x}+\frac{\partial v_x}{\partial y}\right)\right]\right)+\tau_{b,y}=\rho g H\frac{\partial h}{\partial y}, \end{aligned} \tag{1}$$

where v_x and v_y are the velocity components in x- and y-direction, respectively, H is the ice thickness, $h=H+b$ the ice-surface elevation with ice-base elevation b, ρ is the ice density, g the gravitational acceleration and n denotes Glen's flow-law exponent~~(, a common choice is $n=3$)~~. The effective strain rate $\dot{\epsilon}_e$ (Greve and Blatter, 2009) can be written as

$$\dot{\epsilon}_e=\left[\left(\frac{\partial v_x}{\partial x}\right)^2+\left(\frac{\partial v_y}{\partial y}\right)^2+\frac{\partial v_x}{\partial x}\frac{\partial v_y}{\partial y}+\frac{1}{4}\left(\frac{\partial v_x}{\partial y}+\frac{\partial v_y}{\partial x}\right)^2\right]^{1/2} \tag{2}$$

We choose the basal shear stress in Eqs. (1), $\boldsymbol{\tau}_b=(\tau_{b,x},\tau_{b,y})$, to be given by a Weertman-type sliding law (Greve and Blatter, 2009):

$$\boldsymbol{\tau}_b=-C|\boldsymbol{v}|^{m-1}\boldsymbol{v}, \tag{3}$$

with horizontal velocity vector $\boldsymbol{v}=(v_x,v_y)$ and constant friction coefficient C. The exponent m determines the particular type of the sliding law including plastic ($m=0$, magnitude of basal shear stress independent of velocity, Tulaczyk et al., 2000) and linear-viscous ($m=1$, basal shear stress proportional to ice velocity, MacAyeal, 1989) behavior. A value of $m=1/n=1/3$ is commonly assumed to represent sliding over rough bed (Schoof, 2007a; Joughin et al., 2009; Cuffey and Paterson, 2010).

The evolution equation for the ice thickness, i.e., the ice thickness equation (ITE), which results out of mass conservation (Greve and Blatter, 2009) reads

$$\frac{\partial H}{\partial t}=-\mathrm{div}\,\boldsymbol{Q}+a, \tag{4}$$

with horizontal ice flux $\boldsymbol{Q}=H\boldsymbol{v}$ and surface mass balance a. Throughout the study we focus on the grounded part of the ice sheet and assume negligible melting/refreezing at its base. Hence the basal mass balance is not taken into account in Eq. (4).

2.2 Flow-line case

In the flow-line case the geometry of an ice sheet can be scaled in horizontal (x) and vertical (z) direction, using two scaling factors α and β, respectively ($\alpha,\beta>1$ for ~~stretching and $\alpha,\beta<1$ for compression~~elongation and $0<\alpha,\beta<1$ for shortening). We define these as

$$x'=\alpha x, \tag{5}$$

$$h'(x')=H'(x')+b'(x')=\beta H(x)+\beta b(x)=\beta h(x), \tag{6}$$

where the prime denotes the scaled system. In particular, Eq. (5) states that the ice-sheet length L scales according to $L'=\alpha L$.

Since we neglect the y-direction here, we only have to consider the x-component of the SSA (Eq. 1a) in which all terms that include y drop out. The effective strain rate (Eq. 2) thus simplifies to $\dot{\epsilon}_e=\left|\frac{\partial v_x}{\partial x}\right|$ and the SSA reads

$$2A^{-1/n}\frac{\partial}{\partial x}\left[H\left|\frac{\partial v_x}{\partial x}\right|^{1/n-1}\frac{\partial v_x}{\partial x}\right]-Cv_x^m-\rho gH\frac{\partial(H+b)}{\partial x}=0. \tag{7}$$

The ITE (Eq. 4) in flow line is given by

$$\frac{\partial H}{\partial t}=-\frac{\partial(Hv_x)}{\partial x}+a. \tag{8}$$

Now we bring these two equations into non-dimensionalized form by introducing the dimensionless variables $H^*=\frac{H}{\mathcal{H}}$, $b^*=\frac{b}{\mathcal{H}}$ and $v_x^*=\frac{v_x\mathcal{T}}{\mathcal{L}}$, using the scales $\mathcal{H}$, $\mathcal{L}$ and $\mathcal{T}$ for ice-sheet thickness, length and response time, respectively. We obtain

$$\begin{aligned} &\underbrace{\frac{2A^{-1/n}\mathcal{T}^{-1/n}}{\rho g\mathcal{H}}}_{=\theta}\frac{\partial}{\partial x^*}\left[H^*\left|\frac{\partial v_x^*}{\partial x^*}\right|^{1/n-1}\frac{\partial v_x^*}{\partial x^*}\right]\\ &-\underbrace{\frac{C\mathcal{L}^{m+1}\mathcal{T}^{-m}}{\rho g\mathcal{H}^2}}_{=\phi}v_x^{*m}-H^*\frac{\partial(H^*+b^*)}{\partial x^*}=0, \end{aligned} \tag{9}$$

and

$$\frac{\partial H^*}{\partial t^*}=-\frac{\partial(H^*v_x^*)}{\partial x^*}+\underbrace{\frac{a\mathcal{T}}{\mathcal{H}}}_{=\omega}, \tag{10}$$

for the SSA and ITE, respectively. In Eq. (9) the two dimensionless constants θ and ϕ relate the different involved stresses to the driving stress. Extending θ with $\mathcal{H}/\mathcal{L}$ and ϕ with $\mathcal{L}^{-1}$ we see that these scale factors ~~relates~~ relate the membrane stresses (Hindmarsh, 2006) and the basal stresses to the driving stress, respectively. ~~Here we do not assume one of the limits for which~~ In the floating ice shelf the driving stress is ~~either fully supported by~~ always fully balanced by the membrane stresses (~~$\phi\ll\theta$, situation in an ice shelf) or basal shear stresses ($\phi\gg\theta$, holding for ice frozen to bedrock), respectively, but consider the general case in which non of the stress balance terms are neglected~~no basal resistance, thus $C=0$ in Eq. 9). Focussing on the

grounded part of the ice sheet, we assume that its driving stress is balanced by a combination of membrane stresses and basal stresses.

The two governing equations (9) and (10) of our problem remain exactly the same as long as each of the dimensionless factors θ, ϕ and ω ~~are kept constant~~remain the same. In other words, the ice-sheet dynamics are expected to be similar under a transformation that leaves these factors unchanged. Thus the scaling of the ice sheet's typical length and thickness scales according to Eqs. (5) and (6), i.e., $\mathcal{L}' = \alpha\mathcal{L}$ and $\mathcal{H}' = \beta\mathcal{H}$ in general requires (some of) the physical parameters a, C, A and its response time $\mathcal{T}$ to change in order to maintain similarity with respect to the unscaled ice sheet. We hence can infer three scaling conditions for the time-scale ratio $\tau = \mathcal{T}'/\mathcal{T}$:

$$\phi' = \phi \quad \Rightarrow \quad \tau = \alpha^{1+1/m}\beta^{-2/m}\gamma^{1/m}, \tag{11}$$

$$\theta' = \theta \quad \Rightarrow \quad \tau = \beta^{-n}\zeta^{-1}, \tag{12}$$

$$\omega' = \omega \quad \Rightarrow \quad \tau = \beta\delta^{-1}, \tag{13}$$

with friction-coefficient ratio $\gamma = C'/C$, ice-softness ratio $\zeta = A'/A$ and surface-mass-balance ratio $\delta = a'/a$. This system of 3 equations has 6 unknowns from which 4 remain when we take α and β as given by the applied geometric transformation. Prescribing one of the three parameter ratios γ, δ or ζ hence determines the scaling of the other two parameters and the time scaling of the system.

We can link the ratios of surface mass balance and ice softness by combining Eqs. (12) and (13), yielding

$$\delta = \beta^{n+1}\zeta, \tag{14}$$

a relation which is independent of the horizontal scaling factor α. For the case of a scaled ice-sheet geometry that is left unchanged in vertical direction ($\beta = 1$) ice softness and accumulation hence scale identically.

Using Eqs. (11)-(13) we can further express δ and ζ as functions of both geometric scaling ratios and the basal friction ratio:

$$\delta = \alpha^{-(1+1/m)}\beta^{1+2/m}\gamma^{-1/m}. \tag{15}$$

$$\zeta = \alpha^{-(1+1/m)}\beta^{-n+2/m}\gamma^{-1/m}. \tag{16}$$

Inserting Eq. (14) into Eq. (16) we also obtain a condition for the basal-friction ratio as a function of both geometric scaling parameters and the surface-mass-balance ratio:

$$\gamma = \alpha^{-(1+m)}\beta^{2+m}\delta^{-m}. \tag{17}$$

Results of an application of the derived scaling laws in numerical flow-line simulations are given in Sec. 3

2.3 Consistency with flow-line boundary-layer theory

Here we show that the scaling conditions derived above by dimensional analysis under the concept of similitude ~~,~~are consistent with the boundary-layer theory which was introduced by Schoof (2007b) for ~~an~~ a steady-state, unbuttressed, isothermal, flow-line ice sheet in SSA. Neglecting membrane stresses in the SSA stress balance, matched asymptotics are applied to solve a boundary-layer problem for the transition zone between grounded and floating ice. ~~The~~ This theory thus applies further assumptions to the SSA and ITE compared to the more general versions of these equations that are used in the present study.

According to the boundary-layer theory the ice-sheet surface slope is ~~then~~ given by (Schoof, 2007b, Eq. 25)

$$\frac{\partial h(x)}{\partial x} = \frac{\partial(H(x)+b(x))}{\partial x} = \frac{C}{\rho g}\frac{|Q(x_{gl})|^{m-1}Q(x_{gl})}{h(x)^{m+1}}, \tag{18}$$

where x_{gl} denotes the grounding-line position and $Q(x_{gl})$ is the flux across the grounding line. According to Eqs. (5) and (6) the scaling of the surface slope reads

$$\frac{\partial h'(x')}{\partial x'} = \frac{\beta}{\alpha}\frac{\partial h(x)}{\partial x} \tag{19}$$

and in combination with Eq. (18) we can write

$$\frac{C'}{\rho g}\frac{\left|Q'(x'_{gl})\right|^{m-1}Q'(x'_{gl})}{h'(x')^{m+1}} = \frac{\beta}{\alpha}\frac{C}{\rho g}\frac{|Q(x_{gl})|^{m-1}Q'(x_{gl})}{h(x)^{m+1}}. \tag{20}$$

Presuming that the flux across the grounding line is always positive in x-direction and using once again Eq. (6) yields a scaling relation for the grounding-line flux

$$Q'(x'_{gl}) = \alpha^{-1/m}\beta^{(1+2/m)}\gamma^{-1/m}Q(x_{gl}). \tag{21}$$

The boundary-layer method considers the ITE in steady state ($\frac{\partial H}{\partial t} = 0$) and hence integration of ~~(~~Eq. (4) over the entire ~~ice-sheet length~~ length of the grounded ice sheet yields

$$Q(x_{gl}) = aL. \tag{22}$$

Inserting this expression for the grounding-line flux into Eq. (21) we arrive at the same condition for the scaling of the surface mass balance (Eq. 15) that we obtained from the principle of similitude in the previous section.

A central result of the ~~boundary layer~~ boundary-layer theory is an analytic solution for the grounding-line flux as a function of ice thickness at the grounding line ~~(Schoof2007, Eq. (16))~~(Schoof, 2007b, Eq. 16):

$$Q(x_{gl}) = \left(\frac{A(\rho g)^{1+n}(1-\rho/\rho_w)^n}{4^n C}\right)^{\frac{1}{m+1}} H(x_{gl})^{\frac{m+n+3}{m+1}}. \tag{23}$$

Inserting this relation into Eq. (21) and applying some basic algebra we obtain the same scaling relation for the ice softness as derived in the previous sections (Eq. 16).

Setting $Q(x_{gl}) = v_x(x_{gl})H(x_{gl})$ in Eq. (22) and dividing by $Q'(x_{gl})$ we obtain

$$\frac{v_x'(x_{gl}')}{v_x(x_{gl})} = \alpha\beta^{-1}\delta. \tag{24}$$

Since the boundary-layer theory assumes steady-state conditions, we introduce a velocity scale $\mathcal{V} = \mathcal{L}/\mathcal{T}$ to be able to derive a response-time relation. This yields $v_x'/v_x = \alpha/\tau$ and the response-time scaling law resulting from Eq. (24) is identical to Eq. (13).

Thus the same 3 independent equations that determine the ice-sheet scaling behavior and were derived by the means of similarity analysis in the previous section also result from boundary-layer theory.

2.4 Two-dimensional case with one time and one length scale

The two-dimensional SSA (Eq. 1) is derived from the full-Stokes equation using a single horizontal length scale $\mathcal{L}$ and time scale $\mathcal{T}$, respectively (Greve and Blatter, 2009). Continuing this line of thought, we introduce the dimensionless velocity in y-direction, $v_y^* = \frac{v_y \mathcal{T}}{\mathcal{L}}$, in addition to the dimensionless variables from Sec. 2.2 to non-dimensionalize the SSA equations. The dimensionless effective strain rate (Eq. 2) then reads

$$\dot{\epsilon}_e^* = \mathcal{T}\dot{\epsilon}_e \tag{25}$$

For the x-component of the SSA (Eq. 1a) we hence obtain

$$\underbrace{\frac{A^{-1/n}\mathcal{T}^{-1/n}}{\rho g \mathcal{H}}}_{=\Theta}\left(\frac{\partial}{\partial x^*}\left[\dot{\epsilon}_e{}^{*1/n-1} H^* \left(2\frac{\partial v_x^*}{\partial x^*} + \frac{\partial v_y^*}{\partial y^*}\right)\right]\right.$$
$$\left. + \frac{1}{2}\frac{\partial}{\partial y^*}\left[\dot{\epsilon}_e{}^{*(1-n)/n} H^* \left(\frac{\partial v_x^*}{\partial y^*} + \frac{\partial v_y^*}{\partial x^*}\right)\right]\right)$$
$$- \underbrace{\frac{C\mathcal{L}^{m+1}\mathcal{T}^{-m}}{\rho g \mathcal{H}^2}}_{=\Phi} v_x{}^{*m} - H^*\frac{\partial(h^*+b^*)}{\partial x^*} = 0. \tag{26}$$

The same coefficients Θ and Φ result from the y-component of the SSA, which is not specified here. The non-dimensionalized ITE (Eq. 4) reads

$$\frac{\partial H^*}{\partial t^*} = -\mathrm{div}\,(H^*\boldsymbol{v}^*) + \underbrace{\frac{a\mathcal{T}}{\mathcal{H}}}_{=\Omega}. \tag{27}$$

Comparison between the flow-line and the two-dimensional SSA and ITE shows that we obtained the same number of dimensionless factors that appear at the same place and are identical to each other, i.e., $\theta = \Theta$, $\phi = \Phi$ and $\omega = \Omega$. Hence under the assumption of a single horizontal length scale the scaling relations for the two-dimensional SSA are the same as in the flow-line case.

2.5 Two-dimensional case with time and length scales for both horizontal directions

Starting again from the two-dimensional SSA (Eq. 1) we now make the less-constraining assumption of two horizontal length scales $\mathcal{L}_x$ and $\mathcal{L}_y$ and accordingly two time scales $\mathcal{T}_x$ and $\mathcal{T}_y$, yielding the dimensionless velocities $v_x^* = \frac{v_x \mathcal{T}_x}{\mathcal{L}_x}$ and $v_y^* = \frac{v_y \mathcal{T}_y}{\mathcal{L}_y}$. In this case the effective strain rate (Eq. 2) does not simplify to a single term as in the previous sections but consists of several mixed terms. The SSA thus expands to a much longer expression which we detail in the Appendix A. Although we obtain a multiple of dimensionless coefficients that need to remain ~~constant~~ the same for the ice sheet to fulfill similarity under scaling, the resulting scaling laws are identical to the ones derived above (see Appendix A). This implies that our requirement of similarity results in the constraint that the ice sheet can have only one time scale $\mathcal{T} = \mathcal{T}_x = \mathcal{T}_y$ and one length scale $\mathcal{L} = \mathcal{L}_x = \mathcal{L}_y$ as opposed to our initial assumption of distinct scales for each horizontal direction.

We investigate ice-sheet scaling also in a three-dimensional setup in the next section.

3 Comparison with simulations

We compare our analytical findings with results from numerical simulations applying the Parallel Ice Sheet Model in conceptual geometric setups. The model is the same as used in (Feldmann and Levermann, 2015a) but here run in SSA-only mode. We define a reference topographic geometry which is prescribed in an unscaled reference experiment (indexed as "ref") along with the parameter values shown in Table 1. The scaling experiments use geometrically scaled versions of the reference bed topography and the physical parameters are modified according to the scaling laws derived in Sec. 2.2.

Halfing the horizontal and/or vertical length scales of the reference topography we obtain three geometric configurations which are ~~shrinked~~ shortened in vertical $(\alpha, \beta) = (1.0, 0.5)$, horizontal $(\alpha, \beta) = (0.5, 1.0)$ or both directions $(\alpha, \beta) = (0.5, 0.5)$, respectively. To be able to calculate the other physical parameters a, A, C that apply to the scaling experiments according to the 3 scaling relations (Eqs. 15 - 17) we need to prescribe one more scaling ratio in addition to α and β. Setting $\gamma = 1$ (~~constant~~ identical basal friction) and $\delta = 1$ (~~constant~~ identical surface mass balance), thus two sub-sets of simulations are generated. The resulting scaling ratios which determine the parameter values are shown in Table 2 for each of the seven experiments. We apply the described procedure using 1) a flow-line setup (one horizontal and one vertical direction, bed topography in black in Fig. 2) and 2) a three-dimensional channel-flow setup (flow-line setup extended ~~by~~ into second horizontal direction ~~, bed topography shown in Figs. 3 and 4)as detailed~~ with

valley-shaped bedrock in this direction to form a bed trough, see Fig. 4). Details are given in Appendix B.

The experiments are designed to perturb an ice sheet in equilibrium, triggering a marine ice-sheet instability that unfolds unaffected by the ceased perturbation. The speed of unstable grounding-line retreat and the equilibrium ice-sheet profiles before and after the instability serve as a measure to compare the scaling of the dynamic response and the steady-state geometry, respectively.

3.1 Comparing time scales of instability

All of our simulations show a similar pattern of grounding-line evolution after perturbation (Figs. 5 and 6): ~~After~~ after a phase of little to negligible grounding-line retreat the retreat rate increases (grounding line passes the coastal sill and enters the retrograde slope), reaching its maximum value around the minimum of the bed depression before declining to zero (grounding line stabilizes on inland up-sloping bed). The initial and final grounding-line positions of comparable setups (continuous lines) match or are close to each other. The similarity of ice-sheet shapes between different geometric configurations becomes apparent when laying the modeled steady-state ice-sheet profiles on top of each other and scaling the spatial axes according to α and β (shown exemplarily in Figs. 2 and 3).

The simulations clearly differ in the time scale of the MISI evolution which can be measured by the grounding-line retreat rate $\dot{x}_{gl} = \frac{\partial x_{gl}}{\partial t}$. To compare different simulations we introduce a retreat-rate scaling ratio:

$$\dot{\chi} = \frac{\dot{x}'_{gl}}{\dot{x}_{gl}} = \frac{\alpha}{\tau}. \tag{28}$$

Dependent on which additional parameter is ~~held constant~~ prescribed to be identical under geometric scaling, we replace the time-scale ratio using Eq. (11) or Eq. (13) to obtain scaling laws for the retreat rate as functions of the geometric scaling ratios only:

$$\gamma = 1 \quad \Rightarrow \quad \dot{\chi} = \alpha^{-1/m}\beta^{2/m}, \tag{29}$$

$$\delta = 1 \quad \Rightarrow \quad \dot{\chi} = \alpha\beta^{-1}. \tag{30}$$

We can thus calculate the retreat-rate ratios for all considered geometric configurations (Table 2). The grounding-line curves of our simulations are approximately linear over the time period during which the grounding line passes the bed depression and its retreat rate is largest. We fit a slope to the linear section of the unscaled simulation (purple slope fitted to black curve in Figs. 5 and 6), to obtain our reference retreat rate. Using the calculated retreat-rate ratios from Table 2 we can predict the grounding-line retreat rates for the scaled setups. Superimposing the linear sections of the scaled experiments with the respective analytically calculated slope (Figs. 5 and 6) gives a good match between numerical results and theory (see Figs. C1 and C2 for scaled versions of the time series). Our simulation ensemble of scaled ice sheets thus exhibits similarity as predicted from theory, regarding transient ice-sheet dynamics and steady-state geometry.

4 Implications for the response times of ice sheets

Based on the scaling laws derived in Sec. 2 we explore analytically the implications of a scaling of ice-sheet parameters and geometry for the response-time scaling. Making the assumption ~~of a constant~~ that the basal friction parameter stays the same ($\gamma = 1$) while allowing ~~a variation in~~ different values for the surface mass balance and the ice softness we are able to calculate the response-time ratio τ (Eq. 11) as a function that only depends on the geometric scaling (α and β) and the friction exponent m:

$$\tau = \alpha^{1+1/m}\beta^{-2/m}. \tag{31}$$

Using this equation in combination with Eqs. (12) and (13) we obtain contour maps for the ratios τ, ζ and δ in the α-β phase space ~~(Figs. 7a-c for the common choice of an exponent value of $m = 1/n$ with $n = 3$~~ (Figs. 7a-c for the common choice of an exponent value of $m = 1/n$ with $n = 3$ Schoof, 2007a; Greve and Blatter, 2009; Cuffey and Paterson, 2010). Therein the blue and red areas correspond to the regimes of an increasing and decreasing parameter value under geometric scaling, respectively, which are separated by a white curve along which the considered parameter remains ~~constant~~the same.

4.1 Linking horizontal and vertical scales

To be able to follow physically motivated curves through the phase space we link the horizontal and the vertical scale. ~~Motivated by~~ In idealized flow-line experiments (Feldmann and Levermann, 2015a) it has been shown that the Vialov ice-sheet profile (Vialov, 1958; Greve and Blatter, 2009), though derived under the assumption of the shallow-ice approximation, can be used to also approximate SSA ice-sheet profiles. Motivated by the Vialov profile, for which the central (maximum) ice-sheet thickness is proportional to the square root of the ice-sheet length, we assume a relation between the ice-thickness scale $\mathcal{H}$ and the length scale $\mathcal{L}$ of the form

$$\mathcal{H} \sim \mathcal{L}^q \quad \text{with} \quad 0 < q \leq 1. \tag{32}$$

With $\alpha = \mathcal{L}'/\mathcal{L}$ and $\beta = \mathcal{H}'/\mathcal{H}$ it follows that for the postulated ice-sheet proportion the two geometric scaling factors are linked such that

$$\beta = \alpha^q, \tag{33}$$

and Eq. (31) then reads

$$\tau = \alpha^{\frac{m-2q+1}{m}}. \tag{34}$$

We are interested in finding a critical value of the exponent in Eq. (31) which determines a threshold in the α-β phase space between the two regimes of increasing ($\tau < 1$) and decreasing ($\tau > 1$) ice-sheet response time under applied geometric scaling. Assuming horizontal ~~stretching~~ elongation ($\alpha > 1$), which according to Eq. (33) implies also vertical ~~stretching~~ elongation ($\beta > 1$, see Fig. 7d), it follows that $\tau < 1$ only if the exponent in Eq. (34) is negative. Hence there exists a critical threshold

$$q_c = \frac{m+1}{2}, \tag{35}$$

with $m \in (0, 1]$ and thus $q_c \in (\frac{1}{2}, 1]$, above which the scaled, i.e. ~~stretched~~elongated, system responds faster compared to the unscaled system. This is visualized in Fig. 7a for $m = 1/3$. The area between the dashed ($q = q_c = 2/3$) and the continuous ($q = 1$) curves is in the regime of $\tau < 1$ for $\alpha > 1$. Vice versa, for a ~~shrinked~~ shortened ice sheet ($\alpha < 1$ and hence $\beta < 1$) in the area between these two curves holds $\tau > 1$. The same qualitative scaling applies to the ice softness whereas the surface mass balance scales oppositely (Figs. 7b and c).

An exponent of $q = 1/2$ which represents Vialov proportions constitutes the lower aymptotic limit of the domain of all possible q_c (limit $m \to 0$, Eq. 34 requires $m > 0$ for α to remain finite). Thus a Vialov-shaped ice sheet exhibits a response-time scaling oppositely to the scaling explained above (the dotted Vialov curve in Fig. 7a lies always outside the region between continuous and dahed curve, independently of m).

Assuming Vialov conditions under ~~constant~~ identical friction, the scaling of the response time (Eq. 31), surface mass balance (Eq. 15) and ice softness (Eq. 16), respectively, becomes independent of m which is visualized in Fig 8. Evaluating the curves in the left vicinity of $\alpha = 1$, meaning a small reduction in both vertical and horizontal ice-sheet extent, yields a plausible scaling of the ice-sheet parameters in a warming atmosphere: ~~Rising~~ rising atmospheric temperatures cause an increase in surface mass balance ($\delta > 1$ in Fig. 7c, Frieler et al., 2015) and also lead to a softening of the ice ($\zeta > 1$ in Fig. 7b, Cuffey and Paterson, 2010). The response time then decreases ($\tau < 1$ in Fig. 7a). In this picture a warming-induced ice-sheet retreat would hence shift the ice sheet into the regime of faster response to perturbation, tending to accelerate potential further retreat.

4.2 Role of basal friction exponent m

The response-time scaling considered here is a function of the basal friction exponent m (Eq. 31) and the visualization of the response-time ratio in the α-β phase space (Fig. 7 accounts for only one value of m). To examine the influence of m on the scaling we cut several hypersurfaces through the phase space, sampling the domain of the exponent.

Fixing the horizontal scale, i.e., going along $\alpha = 1$, yields that vertical ~~stretching (shrinking~~elongation (shortening) always results in a ~~short~~ shorter (longer) ice-sheet response time (Fig. 9a). In this case the parameter choice of m only determines the curvature of $\tau(\beta)$. Fixing the vertical scale ($\beta = 1$) results in opposite behavior of τ, i.e., horizontal ~~stretching (shrinking~~elongation (shortening) always yields a longer (shorter) ice-sheet response time (Fig. 9b). Equal geometric scaling of the two directions ($\alpha = \beta$) gives a similiar picture as obtained for $\alpha = 1$ (the magnitude of the negative β-exponent is always larger than the α-exponent), with the difference that here the time scaling becomes independent of the geometric scaling for $m = 1$ (Fig. 9c).

Requiring the response-time scaling law (Eq. 31) to be independent of m yields the relation $\beta = \alpha^{\frac{1-m(k-1)}{2}}$ (with k a real number) and thus $\tau = \alpha^k$. In general, a negative (positive) value of k then results in a faster (slower) response when ~~stretching (shrinking~~elongating (shortening) the ice sheet horizontally. The case of $k = 0$ yields ~~a constant~~ the same time scale ($\tau = 1$), independent of the α value (Fig. 9d). The case of $k = 1$ corresponds to the Vialov case for which the time-scale ratio increases linearly when ~~stretching~~ elongating the ice sheet horizontally.

5 Discussion and conclusions

Carrying out a dimensional analysis of the stress balance in SSA and the equation of mass conservation we derive ice-sheet scaling conditions for the vertical and horizontal length scales, the response time and the relevant physical parameters which determine ice-sheet behavior.

Specifically, we find that the scaling relations derived for the SSA in flow line (Eqs. 11-13) also hold for the SSA in two horizontal dimensions under the ~~assumtion~~ assumption of a single horizontal time ~~and length scale, respectively~~scale and a single length scale. Only the two-dimensional SSA accounts for stress components that allow for horizontal shearing and hence the effect of buttressing.

Our analysis also shows that although the full SSA accounts for both horizontal dimensions there can only exist one time scale $\mathcal{T}$ and one length scale $\mathcal{L}$, as opposed to one for each dimension ($\mathcal{T}_x$, $\mathcal{T}_y$ and $\mathcal{L}_x$, $\mathcal{L}_y$) under the principle of similitude.

To non-dimensionalize the SSA stress balance we introduce scales for ice-sheet length, thickness and time without assuming typical numerical values for these scales. We thus do not ~~compare orders of magnitudes of acting stresses to neglect~~ neglect further terms in the ~~stress balance as is often done in the course of a dimensional analysis (citation)~~ SSA stress balance by comparing orders of magnitudes of acting stresses (as done in, e.g., Schoof, 2007a) but consider the general case ~~of comparable magnitudes of~~ in which both membrane and basal stresses ~~, respectively~~ balance the driving stress (Eqs. 9 and 26). In other studies ~~not only~~ the scales for ice-sheet ~~length, thicknessand velocity but also~~ thickness, length and time are used to express the friction pa-

rameter C ~~is expressed by typical scales of length, thickness and time~~ resulting in a dimensionless SSA stress balance that is characterized by a single scaling parameter (often denoted as ϵ, Schoof, 2007a; Tsai et al., 2015). In the present study we consider C as an independent parameter/scale and thus obtain two scaling parameters θ and ϕ in the ~~stress balance (Eqs. 9 and 26)~~SSA stress balance. The resulting scaling laws hence involve the scaling of the basal roughness explicitely. The same holds for the scaling of the surface mass balance a.

The scaling laws derived here are consistent with boundary-layer theory which considers the transition zone between the grounded and floating regimes of a rapidly sliding equilibrium ice sheet in flow line (Schoof, 2007b). The conditions that don't involve a time scale (Eqs. 15 and 16) follow directly out of the analytic equations for steady-state ice-sheet geometry and the grounding-line flux that result from boundary-layer theory. To obtain the scaling relation also for the ice-sheet response time (Eq. 13) out of the steady-state theory it is necessary to introduce a velocity scale.

The presented scaling conditions can provide rules in the design of model setups for numerical simulations as well as laboratory experiments to obtain parameter sets that leave the ice-sheet geometry (~~absolute~~ shape and extent) unchanged. For instance, a doubling of the basal-friction parameter under ~~constant~~ identical surface mass balance requires the ice softness to be reduced to 1/8 (Eqs. 14 and 15), or a doubling in surface mass balance under ~~constant~~ identical basal friction requires a doubling of the ice-softness value (Eqs. 15). Note that these equations by no means make a statement about the physical dependency between ice softness, basal friction or surface mass balance. Our results, derived under the principle of similitude, provide conditions that have to be fulfilled in order to respect self-similarity of idealized ice sheets. In other words: if two (idealized) glaciers, that are in equilibrium with their environment and the SSA equation, have the same qualitative shape but differ, e.g., in surface mass balance then they also need to differ in basal friction and their specific relation is given by the scaling conditions.

For the numerical simulations conducted in this study we apply parameter configurations that half the geometric scale in horizontal and/or vertical direction with respect to the reference. The resulting ice-sheet response times range over three orders of magnitude (see Table 2). Irrespective of whether in a two- or three-dimensional setup the modeled ice-sheet dynamics, represented by the rate of unstable grounding-line retreat (Figs. 5 and 6) as well as the geometry, represented by ice-sheet shape and grounding line position in equilibrium (Figs. 2 – 4), exhibit the scaling behavior predicted from the analytical calculations to a good approximation. For the flow-line setup three scaled parameter sets show different qualitative ice-sheet evolution compared to the reference, while still complying with the expected response-time scaling. This difference is attributed to the design of the reference setup, i.e., the closeness of the initial steady-state grounding line to the point of instability (local bed maximum). Very small deviations from this position trigger unperturbed instability or prevent landward induced instability in the scaled setups (see Appendix B).

In contrast to the flow-line configuration the three-dimensional setup inherently accounts for the buttressing effect in the initial steady-state simulation due to the presence of a confined ice shelf (Dupont and Alley, 2005; Gudmundsson et al., 2012). However, the ice shelf is removed in the course of perturbation to prevent scale-dependent influences that would originate from a forcing through sub-shelf melting, surface accumulation or ice softness. Thus the speed of grounding line retreat (and hence ice-sheet response time) is only indirectly affected by the former buttressing effect. An investigation of the response-time scaling under direct influence of ice-shelf buttressing requires a carefully designed experimental setup that maintains the ice shelf during perturbation (as in Asay-Davis et al., 2015) and accounts for the scaling also in the applied forcing.

To analytically investigate the implications of geometric scaling for the ice-sheet response time we make the simplifying assumption of ~~constant~~ identical basal friction ($\gamma = 1$). Though the response-time scaling law ~~still~~ then still depends on the sliding exponent m (Eq. 31) the qualitative response-time scaling (shorter or longer response time) turns out to be independent of the choice of m (Fig. 9): ~~Vertical~~ vertical ice-sheet ~~stretching (compression~~elongation (shortening) leads to a faster (slower) ice-sheet response and the opposite holds for the horizontal direction. In other words, thicker or shorter ice sheets tend to respond faster than thinner or longer ones. Equal scaling in horizontal and vertical direction ($\alpha = \beta$) yields that larger ice sheets respond faster than smaller ones.

Assuming a relation between the horizontal and vertical scale of the form $\beta = \alpha^q$ with $0 < q \leq 1$, we find a critical m-dependent threshold q_c for the exponent (Eq. 35) above which larger (smaller) ice sheets always exhibit a shorter (longer) response time. The case of $q = 1/2$ represents the lower asymptotic limit for all possible q_c and corresponds to an ice sheet with Vialov-type proportions for which the central ice thickness is the square root of the horizontal extent. Conceptual flow-line experiments similar to the ones conducted here (Feldmann and Levermann, 2015a) revealed that the Vialov profile, which results under simplified conditions from the ~~shallow-ice approximation~~ SIA of the full-Stokes stress balance in flow line, can also ~~reasonable~~ reasonably approximate the ice-sheet shape in SSA. In the same study a comparison between steady-state ice-sheet profiles before and after collapse suggested a scaling of $\beta = \alpha^{1/2}$. For such an ice sheet the time scaling is identical to the scaling of its length, i.e., ~~stretching (compression~~elongation (shortening) results in slower (faster) response which is opposite behavior than for the above discussed case of $q > q_c > 1/2$. A thought experiment that is consistent with the scaling behavior derived for this kind of profile reveals that in the course of an ice-sheet retreat that is triggered by atmospheric warm-

ing the ice-sheet response would become faster, with self-accelerating effect on further retreat (Fig 8). Note that all the consideration made above presume self-similarity of ice sheets and are only valid for a ~~constant~~ fixed basal-friction parameter.

In place of prescribing basal friction, the assumption of ~~a constant~~ identical surface mass balance ($\delta = 1$) or ice softness ($\zeta = 1$), results in a more trivial response-time scaling which either equals the vertical scaling (Eq. 13) or depends on the vertical scaling via a power-law relation with exponent $-n$ (Eq. 12), respectively. Since n is always positive ~~also here the qualitative time scaling does not depend on the parameter value~~(Cuffey and Paterson, 2010) in the latter case the response time decreases with increasing vertical extent. There are several other ways to analyze the implications of the scaling conditions derived here on ice-sheet dynamics that are not covered in this study.

Our approach includes several assumptions (shallow stress balance, isothermal ice~~flow~~, choice of sliding law, parameter constraints) and thus simplifies the problem of ice ~~sheet~~ flow. At the same time it allows for the fundamental scaling analysis conducted here which incorporates the relevant physics of fast ice flow and results in scaling conditions that relate important physical parameters of an ice sheet to each other. A similitude analysis based on a less simplified stress balance than the one used here would certainly better account for the complexity of real-world systems, but is beyond the scope of the current study. All statements on the ice-sheet scaling behavior made here therefore need to be considered in the light of the idealized character of the underlying simplified SSA stress balance.

The SSA is of vertically-integrated form and thus in particular does not account for variations of ice-sheet velocity within the ice column. The assumption of uniform ice softness further reduces complexity, neglecting the dependency of the ice softness on ice temperature which typically varies in horizontal and vertical direction. The applied Weertman-type sliding law (Eq. 3) is a common choice (Fowler, 1981; Schoof, 2007a; Pattyn et al., 2013) amongst others used to describe the sliding of ice sheets over bedrock (Greve and Blatter, 2009; Cuffey and Paterson, 2010; Tsai et al., 2015). ~~It~~ Though we prescribe a uniform basal friction coefficient the resulting basal stress field that enters the SSA can vary spatially and temporally. The sliding law covers diverse types of sliding behavior depending on the sliding exponent m in Eq. (31). Except for the plastic limit ($m = 0$) it relates the scale of basal stress to the scale of velocity, resulting in a scaling law which links the scaling of ice-sheet geometry, friction and response time, respectively (Eq. 11).

Our analytic exploration of the derived ice-sheet scaling behavior applies several constraints to the parameter space and is thus far from being holistic but is aimed to allow for (simplified) statements on the influence of geometric scaling on response time. The set of scaling conditions presented here shall provide a model which allows for a fundamental comparison of the large-scale scaling of the geometry and relevant parameters that determine ice-sheet dynamics. In particular the response-time scaling conditions might be suitable to analyze speed of the transient response to climatic perturbations of the polar ice sheets that took place in the past or might become relevant for the future.

Appendix A: Two-dimensional case with two time and length scales for both horizontal directions

Introducing the dimensionless velocities $v_x^* = \frac{v_x \mathcal{T}_x}{\mathcal{L}_x}$ and $v_y^* = \frac{v_y \mathcal{T}_y}{\mathcal{L}_y}$ the non-dimensionalized form of the effective strain rate (Eq. 2) reads

$$\dot{\epsilon}_e = \left[\mathcal{T}_x^{-2} \left(\frac{\partial v_x^*}{\partial x^*} \right)^2 + \mathcal{T}_y^{-2} \left(\frac{\partial v_y^*}{\partial y^*} \right)^2 + \mathcal{T}_x^{-1} \mathcal{T}_y^{-1} \frac{\partial v_x^*}{\partial x^*} \frac{\partial v_y^*}{\partial y^*} + \frac{1}{4} \left(\mathcal{L}_x \mathcal{L}_y^{-1} \mathcal{T}_x^{-1} \frac{\partial v_x^*}{\partial y^*} + \mathcal{L}_x^{-1} \mathcal{L}_y \mathcal{T}_y^{-1} \frac{\partial v_y^*}{\partial x^*} \right)^2 \right]^{1/2}. \tag{A1}$$

Insertion into Eq. (1a) yields the following expression for the x-component of the two-dimensional SSA:

$$\begin{aligned} & \frac{\partial}{\partial x^*} \left[H^* \left(\underbrace{\left[\frac{2A^{-1/n}}{\rho g \mathcal{H} \mathcal{T}_x} \right]^{\frac{2n}{1-n}} \dot{\epsilon}_e^2}_{I} \right)^{\frac{1-n}{2n}} \frac{\partial v_x^*}{\partial x^*} \right. \\ & \left. + H^* \left(\underbrace{\left[\frac{A^{-1/n}}{\rho g \mathcal{H} \mathcal{T}_y} \right]^{\frac{2n}{1-n}} \dot{\epsilon}_e^2}_{II} \right)^{\frac{1-n}{2n}} \frac{\partial v_y^*}{\partial y^*} \right] \\ & + \frac{1}{2} \frac{\partial}{\partial y^*} \left[H^* \left(\underbrace{\left[\frac{A^{-1/n} \mathcal{L}_x^2}{\rho g \mathcal{H} \mathcal{L}_y^2 \mathcal{T}_x} \right]^{\frac{2n}{1-n}} \dot{\epsilon}_e^2}_{III} \right)^{\frac{1-n}{2n}} \frac{\partial v_x^*}{\partial y^*} \right. \\ & \left. + H^* \left(\underbrace{\left[\frac{A^{-1/n}}{\rho g \mathcal{H} \mathcal{T}_y} \right]^{\frac{2n}{1-n}} \dot{\epsilon}_e^2}_{IV} \right)^{\frac{1-n}{2n}} \frac{\partial v_y^*}{\partial x^*} \right] \\ & + \underbrace{\frac{\mathcal{L}_x^{m+1} C}{\rho g \mathcal{H}^2 \mathcal{T}_x^m}}_{=\Phi_x} v_x^{*m} - H^* \frac{\partial (h^* + b^*)}{\partial x^*} = 0, \end{aligned} \tag{A2}$$

with the dimensionless coefficient Φ_x which has the same form as Φ (Eq. 26) but is specific for the x-direction. The terms I, $II = IV$ and III are evaluated in the following to obtain dimensionless factors for the SSA equation. The first

expression I reads:

$$
\begin{aligned}
I = & \underbrace{\left[\frac{2A^{-1/n}}{\rho g \mathcal{H} \mathcal{T}_x^{1/n}}\right]^{\frac{2n}{1-n}}}_{\Theta_{I,1}} \left(\frac{\partial v_x^*}{\partial x^*}\right)^2 \\
& + \underbrace{\left[\frac{2A^{-1/n}}{\rho g \mathcal{H} \mathcal{T}_x \mathcal{T}_y^{\frac{1-n}{n}}}\right]^{\frac{2n}{1-n}}}_{\Theta_{I,2}} \left(\frac{\partial v_y^*}{\partial y^*}\right)^2 \\
& + \underbrace{\left[\frac{2A^{-1/n}}{\rho g \mathcal{H} \mathcal{T}_x^{\frac{1+n}{2n}} \mathcal{T}_y^{\frac{1-n}{2n}}}\right]^{\frac{2n}{1-n}}}_{\Theta_{I,3}} \frac{\partial v_x^*}{\partial x^*} \frac{\partial v_y^*}{\partial y^*} \\
& + \frac{1}{4} \Bigg(\underbrace{\left[\frac{2A^{-1/n}}{\rho g \mathcal{H} \mathcal{T}_x^{1/n}} \left(\frac{\mathcal{L}_x}{\mathcal{L}_y}\right)^{\frac{1-n}{n}}\right]^{\frac{n}{1-n}}}_{\Theta_{I,4}} \frac{\partial v_x^*}{\partial y^*} \\
& + \underbrace{\left[\frac{2A^{-1/n}}{\rho g \mathcal{H} \mathcal{T}_x \mathcal{T}_y^{\frac{1-n}{n}}} \left(\frac{\mathcal{L}_y}{\mathcal{L}_x}\right)^{\frac{1-n}{n}}\right]^{\frac{n}{1-n}}}_{\Theta_{I,5}} \frac{\partial v_y^*}{\partial x^*} \Bigg)^2 ,
\end{aligned}
\tag{A3}
$$

from which we obtain five dimensionless factors $\Theta_{I,1}, ..., \Theta_{I,5}$. Applying the same steps for expressions II and III yields ten more coefficients:

$$II = IV: \quad \Theta_{II,1} = \Theta_{IV,1} = \frac{2A^{-1/n}}{\rho g \mathcal{H} \mathcal{T}_x^{\frac{1-n}{n}} \mathcal{T}_y} \tag{A4}$$

$$\Theta_{II,2} = \Theta_{IV,2} = \frac{2A^{-1/n}}{\rho g \mathcal{H} \mathcal{T}_y^{1/n}} \tag{A5}$$

$$\Theta_{II,3} = \Theta_{IV,3} = \frac{2A^{-1/n}}{\rho g \mathcal{H} \mathcal{T}_x^{\frac{1-n}{2n}} \mathcal{T}_y^{\frac{1+n}{2n}}} \tag{A6}$$

$$\Theta_{II,4} = \Theta_{IV,4} = \frac{2A^{-1/n}}{\rho g \mathcal{H} \mathcal{T}_x^{\frac{1-n}{n}} \mathcal{T}_y} \left(\frac{\mathcal{L}_x}{\mathcal{L}_y}\right)^{\frac{1-n}{n}} \tag{A7}$$

$$\Theta_{II,5} = \Theta_{IV,5} = \frac{2A^{-1/n}}{\rho g \mathcal{H} \mathcal{T}_y^{1/n}} \left(\frac{\mathcal{L}_y}{\mathcal{L}_x}\right)^{\frac{1-n}{n}} \tag{A8}$$

$$III: \quad \Theta_{III,1} = \frac{2A^{-1/n}}{\rho g \mathcal{H} \mathcal{T}_x^{1/n}} \left(\frac{\mathcal{L}_x}{\mathcal{L}_y}\right)^2 \tag{A9}$$

$$\Theta_{III,2} = \frac{2A^{-1/n}}{\rho g \mathcal{H} \mathcal{T}_x \mathcal{T}_y^{\frac{1-n}{n}}} \left(\frac{\mathcal{L}_x}{\mathcal{L}_y}\right)^2 \tag{A10}$$

$$\Theta_{III,3} = \frac{2A^{-1/n}}{\rho g \mathcal{H} \mathcal{T}_x^{\frac{1+n}{2n}} \mathcal{T}_y^{\frac{1-n}{2n}}} \left(\frac{\mathcal{L}_x}{\mathcal{L}_y}\right)^2 \tag{A11}$$

$$\Theta_{III,4} = \frac{2A^{-1/n}}{\rho g \mathcal{H} \mathcal{T}_x^{1/n}} \left(\frac{\mathcal{L}_x}{\mathcal{L}_y}\right)^{\frac{1+n}{n}} \tag{A12}$$

$$\Theta_{III,5} = \frac{2A^{-1/n}}{\rho g \mathcal{H} \mathcal{T}_x \mathcal{T}_y^{\frac{1-n}{n}}} \left(\frac{\mathcal{L}_x}{\mathcal{L}_y}\right)^{\frac{-1+3n}{n}} \tag{A13}$$

In order to obtain the same equations independent of an applied ice-sheet scaling the dimensionless coefficients need to remain ~~constant~~the same. We start with the first set of coefficients:

$$\Theta'_{I,1} \stackrel{!}{=} \Theta_{I,1} \quad \Rightarrow \quad \tau_x = \beta^{-n} \zeta^{-1}, \tag{A14}$$

$$\Theta'_{I,2} \stackrel{!}{=} \Theta_{I,2} \quad \Rightarrow \quad \tau_x = \beta^{-1} \zeta^{-1/n} \tau_y^{-\frac{1-n}{n}}, \tag{A15}$$

$$\Theta'_{I,3} \stackrel{!}{=} \Theta_{I,3} \quad \Rightarrow \quad \tau_x = \beta^{-\frac{2n}{1+n}} \zeta^{-\frac{2}{1+n}} \tau_y^{-\frac{1-n}{1+n}}, \tag{A16}$$

$$\Theta'_{I,4} \stackrel{!}{=} \Theta_{I,4} \quad \Rightarrow \quad \tau_x = \beta^{-n} \zeta^{-1} \left(\frac{\alpha_x}{\alpha_y}\right)^{1-n}, \tag{A17}$$

$$\Theta'_{I,5} \stackrel{!}{=} \Theta_{I,5} \quad \Rightarrow \quad \tau_x = \beta^{-1} \zeta^{-1/n} \left(\frac{\alpha_x}{\alpha_y}\right)^{\frac{1-n}{n}} \tau_y^{-\frac{1-n}{n}}. \tag{A18}$$

We immediately see that Eq. (A14) gives the same time scaling (in x-direction) as derived for the more constraint cases, i.e., in flow-line (Eq. 12) as well as for the two-dimensional case that assumes only one time and length scale, respectively (Sec. 2.4). Comparison of Eqs. (A14) and (A17) directly yields the condition $\alpha_x = \alpha_y$. Furthermore, replacing

β and ζ in Eq. (A15) using Eq. (A14) we obtain $\tau_x = \tau_y$. These two conditions can also be deduced by the comparison of scaling relations that are derived from different coefficients, e.g., $\Theta_{I,1}$,$\Theta_{II,2}$ and $\Theta_{III,1}$. The same procedure can be carried out for the y-component of the SSA leading to the same outcome due to the symmetry of both horizontal components of the SSA. Applying our findings it follows $\Phi_x = \Phi$ in Eq. (A2) and the dimensionless ITE is identical to Eq. ~~27~~ (27) with the same coefficient Ω.

We thus found that in order to fulfill the required scaling similarity in the considered two-dimensional SSA-case there can only exist one horizontal length scale and one time scale (as opposed to one in each horizontal direction, as assumed initially). All the scaling relations derived for the flow-line SSA case (Eqs. 11 - 13) hold here.

Appendix B: Experimental design of numerical simulations

B1 Flow-line simulations

For the two-dimensional simulations, we use the symmetric flow-line geometry and the sequence of experiments described in Feldmann and Levermann (2015a): ~~An~~ an ice sheet in equilibrium (grey profile in Fig.-2) is perturbed in its ~~RHS~~ right-hand-side basin, forcing the grounding line to retreat onto the basin's inward down-sloping bed section (Fig.-2, red profile). After cessation of the perturbation the grounding line continues to retreat indicating that a MISI has been triggered. The resulting far-inland spreading dynamic ice-sheet thinning eventually initiates a second MISI in the connected ~~LHS~~ left-hand-side basin (see Feldmann and Levermann, 2015a, for a detailed examination of the mechanism which is visualized in their Fig. 4a). This second MISI is induced only through internal ice dynamics without any direct forcing and hence we expect that the speed of the instability is a suitable measure to reflect the ice-sheet inherent response time.

For three parameter sets the simulations deviate from the above described scenario. In two simulations ($2D_{\alpha=1,\beta=\frac{1}{2},\delta=1}$ and $2D_{\alpha=\frac{1}{2},\beta=1,\gamma=1}$) the ice sheet does not find a steady state with a grounding-line location on the ocean side of the coastal sill but collapses after several thousand years and equilibrates on the central bed portion. In simulation $2D_{\alpha=1,\beta=\frac{1}{2},\gamma=1}$ only the first MISI is triggered but not the second (referred to as "stable" scenario S in Feldmann and Levermann, 2015a). Though the unstable retreat in these three simulations does not take place as unperturbed as in the scenario described further above we nevertheless use the speed of retreat to estimate ice-sheet response time also for these scaled setups.

B2 Three-dimensional simulations

For the three-dimensional experiments we extend our flow-line geometry by introducing a second horizontal dimension (y) to obtain channel-like ~~ice-sheet~~ ice flow in three dimensions with similar geometry as in Gudmundsson et al. (2012) and Asay-Davis et al. (2015). The bed topography $b(x, y)$ is a superposition of two components: ~~The~~ the bed component in x-direction, $b_x(x)$, is as described in Feldmann and Levermann (2015a) but lowered uniformly by -300 m (Fig. 3). The component in y-direction, $b_y(y)$, is taken from Gudmundsson et al. (2012). The superposition of both, $b(x, y) = b_x + b_y$, yields a bed trough which is symmetric in both x- and y-direction (Fig. 4). While the main ~~ice-sheet~~ ice flow is still in x-direction (from the interior through the bed trough towards the ocean) there is also a flow component in y-direction, i.e., from the channel's lateral ridges down into the trough. Resulting convergent flow and associated horizontal shearing enable the emergence of buttressing, and hence ice dynamics in this setup differ substanitally from the flow-line case. In particular the buttressing effect stabilizes the grounding line further downstream than would be expected in a flow-line configuration (compare Figs. 2 to 3 where the steady-state grounding lines are approximately at the same position but the local bed elevation differs by several 100 m).

Spinning up the model we obtain a symmetric ice sheet in equilibrium with a stable bay-shaped grounding line. Along the centerline of the setup ($y = 0$) the grounding line is located downstream of the coastal sill, similar to the flow-line case (Figs. 4 and 3 in grey). Two symmetric ice shelves have formed which are fringed and fed by ice from the inland and lateral direction. The steady-state ice sheet is then perturbed by removing all floating ice ~~instantaniously~~ instantaneously after which a continuous ~~elemition~~ elimination of all ice that crosses the grounding line is applied. This scaling-independent perturbation initiates grounding-line retreat onto the inland-downsloping bed and the synchronously unfolding MISIs provide a measure for the ice-sheet response time.

Appendix C: Scaled time series of grounding-line retreat

For an alternative comparison of grounding-line retreat rates between the different scaling experiments described in Sec. 3 we plot scaled time series of the grounding line position (Figs. C1 and C2, see Figs. 5 and 6 for the unscaled versions). The scaling is applied along both axes according to the scaling ratios of response time τ and horizontal geometry α that are calculated from theory (Table 2). Focussing on the section of maximum retreat-rate magnitude where the unstable retreat is independent of the applied perturbation, the different curves collapse into a single curve to a good approximation. The scaled speed of the simulated instablities is hence approximately the same, indicating similitude

between the experiments of the scaling ensemble as expected from theory.

References

Alexander, R. M. and Yayes, a. S.: A dynamic similarity hypothesis for the gaits of quadrupedal mamals, Journal of Zoology (London), 201, 135–152, doi:10.1111/j.1469-7998.1983.tb04266.x, http://dx.doi.org/10.1111/j.1469-7998.1983.tb04266.x, 1983.

Asay-Davis, X. S., Cornford, S. L., Durand, G., Galton-Fenzi, B. K., Gladstone, R. M., Gudmundsson, G. H., Hattermann, T., Holland, D. M., Holland, D., Holland, P. R., Martin, D. F., Mathiot, P., Pattyn, F., and Seroussi, H.: Experimental design for three interrelated Marine Ice-Sheet and Ocean Model Intercomparison Projects, Geoscientific Model Development Discussions, 8, 9859–9924, doi:10.5194/gmdd-8-9859-2015, http://www.geosci-model-dev-discuss.net/8/9859/2015/gmdd-8-9859-2015.html, 2015.

Bueler, E. and Brown, J.: Shallow shelf approximation as a "sliding law" in a thermomechanically coupled ice sheet model, Journal of Geophysical Research: Solid Earth, 114, 1–21, doi:10.1029/2008JF001179, 2009.

Bueler, E., Lingle, C. S., ad D. N. Covey, J. a. K.-B., and Bowman, L. N.: Exact solutions and verification of numerical model for isothermal ice sheets, Journal of {G}laciology, 51, 291–306, doi:10.3189/172756505781829449, 2005.

Burton, J. C., Amundson, J. M., Abbot, D. S., Boghosian, A., Cathles, L. M., Correa-Legisos, S., Darnell, K. N., Guttenberg, N., Holland, D. M., and MacAyeal, D. R.: Laboratory investigations of iceberg capsize dynamics, energy dissipation and tsunamigenesis, Journal of Geophysical Research: Earth Surface, 117, 1–13, doi:10.1029/2011JF002055, 2012.

Cornford, S. L., Martin, D. F., Payne, A. J., Ng, E. G., Le Brocq, A. M., Gladstone, R. M., Edwards, T. L., Shannon, S. R., Agosta, C., van den Broeke, M. R., Hellmer, H. H., Krinner, G., Ligtenberg, S. R. M., Timmermann, R., and Vaughan, D. G.: Century-scale simulations of the response of the West Antarctic Ice Sheet to a warming climate, The Cryosphere Discussions, 9, 1887–1942, doi:10.5194/tcd-9-1887-2015, http://www.the-cryosphere-discuss.net/9/1887/2015/tcd-9-1887-2015.html, 2015.

Corti, G., Zeoli, A., and Iandelli, I.: Small-scale modeling of ice flow perturbations induced by sudden ice shelf breakup, Global and Planetary Change, 119, 51–55, doi:10.1016/j.gloplacha.2014.05.002, http://dx.doi.org/10.1016/j.gloplacha.2014.05.002, 2014.

Cuffey, K. M. and Paterson, W. S. B.: The physics of glaciers, 2010.

Dupont, T. K. and Alley, R. B.: Assessment of the importance of ice-shelf buttressing to ice-sheet flow, Geophysical Research Letters, 32, L04 503, doi:10.1029/2004GL022024, http://doi.wiley.com/10.1029/2004GL022024, 2005.

Favier, L., Gagliardini, O., Durand, G., and Zwinger, T.: A three-dimensional full Stokes model of the grounding line dynamics: effect of a pinning point beneath the ice shelf, The Cryosphere, 6, 101–112, doi:10.5194/tc-6-101-2012, http://www.the-cryosphere.net/6/101/2012/, 2012.

Favier, L., Durand, G., Cornford, S. L., Gudmundsson, G. H., Gagliardini, O., Gillet-Chaulet, F., Zwinger, T., Payne, a. J., and Le Brocq, a. M.: Retreat of Pine Island Glacier controlled by marine ice-sheet instability, Nature Climate Change, 5, 117–121, doi:10.1038/nclimate2094, http://www.nature.com/doifinder/10.1038/nclimate2094, 2014.

Feldmann, J. and Levermann, A.: Interaction of marine ice-sheet instabilities in two drainage basins: simple scaling of geometry and transition time, The Cryosphere, 9, 631–645, doi:10.5194/tc-9-631-2015, http://www.the-cryosphere.net/9/631/2015/, 2015a.

Feldmann, J. and Levermann, A.: Collapse of the West Antarctic Ice Sheet after local destabilization of the Amundsen Basin, Proceedings of the National Academy of Sciences, p. 201512482, doi:10.1073/pnas.1512482112, www.pnas.org/cgi/doi/10.1073/pnas.1512482112http://www.pnas.org/lookup/doi/10.1073/pnas.1512482112, 2015b.

Feldmann, J., Albrecht, T., Khroulev, C., Pattyn, F., and Levermann, A.: Resolution-dependent performance of grounding line motion in a shallow model compared with a full-Stokes model according to the MISMIP3d intercomparison, Journal of Glaciology, 60, 353–360, doi:10.3189/2014JoG13J093, 2014.

Fogwill, C. J., Turney, C. S. M., Meissner, K. J., Golledge, N. R., Spence, P., Roberts, J. L., England, M. H., Jones, R. T., and Carter, L.: Testing the sensitivity of the East Antarctic Ice Sheet to Southern Ocean dynamics: past changes and future implications, Journal of Quaternary Science, 29, 91–98, doi:10.1002/jqs.2683, http://doi.wiley.com/10.1002/jqs.2683, 2014.

Fowler, A. C.: A theoretical treatment of the sliding of glaciers in the absence of cavitation, Philosophical Transactions A, 298, 637–681, doi:10.1098/rsta.1981.0003, 1981.

Frieler, K., Clark, P. U., He, F., Buizert, C., Reese, R., Ligtenberg, S. R. M., van den Broeke, M. R., Winkelmann, R., and Levermann, A.: Consistent Evidence of Increasing Antarctic Accumulation With Warming, Nature Climate Change, 5, 348–352, doi:10.1038/nclimate2574, http://www.nature.com.ezproxy.canterbury.ac.nz/nclimate/journal/v5/n4/full/nclimate2574.html, 2015.

Goldberg, D., Holland, D. M., and Schoof, C.: Grounding line movement and ice shelf buttressing in marine ice sheets, Journal of Geophysical Research, 114, F04 026, doi:10.1029/2008JF001227, http://www.agu.org/pubs/crossref/2009/2008JF001227.shtmlhttp://doi.wiley.com/10.1029/2008JF001227, 2009.

Greve, R. and Blatter, H.: Dynamics of Ice Sheets and Glaciers, Advances in Geophysical and Environmental Mechanics and Mathematics, Springer Berlin Heidelberg, Berlin, Heidelberg, doi:10.1007/978-3-642-03415-2, http://openurl.ingenta.com/content/xref?genre=article{&}issn=0022-1430{&}volume=57{&}issue=205{&}spage=981http://link.springer.com/10.1007/978-3-642-03415-2, 2009.

Gudmundsson, G. H., Krug, J., Durand, G., Favier, L., and Gagliardini, O.: The stability of grounding lines on retrograde slopes, The Cryosphere, 6, 1497–1505, doi:10.5194/tc-6-1497-2012, http://www.the-cryosphere.net/6/1497/2012/, 2012.

Halfar, P.: On the dynamics of the ice sheets 2, Journal of Geophysical Research Oceans, 88, 6043–6052, doi:10.1029/JC088iC10p06043, 1983.

Haseloff, M., Schoof, C., and Gagliardini, O.: A boundary layer model for ice stream margins, Journal of Fluid Mechanics, 781, 353–387, doi:10.1017/jfm.2015.503, http://www.journals.cambridge.org/abstract{_}S0022112015005030, 2015.

Hindmarsh, R. C. a.: The role of membrane-like stresses in determining the stability and sensitivity of the Antarctic ice sheets: back pressure and grounding line motion., Philosophical transactions. Series A, Mathematical, physical, and engineering sciences, 364, 1733–67, doi:10.1098/rsta.2006.1797, http://www.ncbi.nlm.nih.gov/pubmed/16782608, 2006.

Hutter, K.: Theoretical Glaciology, Reidel Publ., Dordrecht, Netherlands,, 1983.

Huybrechts, P.: A 3-D model for the Antarctic ice sheet: a sensitivity study on the glacial-interglacial contrast, Climate Dynamics, 5, 79–92, doi:10.1007/BF00207423, 1990.

Joughin, I., Tulaczyk, S., Bamber, J. L., Blankenship, D., Holt, J. W., Scambos, T., and Vaughan, D. G.: Basal conditions for Pine Island and Thwaites Glaciers, West Antarctica, determined using satellite and airborne data, Journal of Glaciology, 55, 245–257, doi:10.3189/002214309788608705, 2009.

Joughin, I., Smith, B. E., and Medley, B.: Marine Ice Sheet Collapse Potentially Under Way for the Thwaites Glacier Basin, West Antarctica, Science, 344, 735–738, doi:10.1126/science.1249055, http://www.sciencemag.org/cgi/doi/10.1126/science.1249055, 2014.

Kundu, P. K., Cohen, I. M., and Dowling, D. R.: Fluid Mechanics, Academic Press, https://books.google.de/books?id=iUo{_}4tsHQYUC, 2012.

Larour, E., Seroussi, H., Morlighem, M., and Rignot, E.: Continental scale, high order, high spatial resolution, ice sheet modeling using the Ice Sheet System Model (ISSM), Journal of Geophysical Research F: Earth Surface, 117, F01 022, doi:10.1029/2011JF002140, http://doi.wiley.com/10.1029/2011JF002140, 2012.

Levermann, A., Clark, P. U., Marzeion, B., Milne, G. A., Pollard, D., Radic, V., and Robinson, A.: The multimillennial sea-level commitment of global warming., Proceedings of the National Academy of Sciences of the United States of America, 110, 13 745–50, doi:10.1073/pnas.1219414110, http://www.scopus.com/inward/record.url?eid=2-s2.0-84882750887{&}partnerID=tZOtx3y1, 2013.

Levermann, A., Winkelmann, R., Nowicki, S., Fastook, J. L., Frieler, K., Greve, R., Hellmer, H. H., Martin, M. a., Meinshausen, M., Mengel, M., Payne, a. J., Pollard, D., Sato, T., Timmermann, R., Wang, W. L., and Bindschadler, R. a.: Projecting Antarctic ice discharge using response functions from SeaRISE ice-sheet models, Earth System Dynamics, 5, 271–293, doi:10.5194/esd-5-271-2014, http://www.earth-syst-dynam.net/5/271/2014/, 2014.

Li, Y., Wu, M., Chen, X., Wang, T., and Liao, H.: Wind-tunnel study of wake galloping of parallel cables on cable-stayed bridges and its suppression, Wind and Structures An International Journal, 16, 249–261, doi:10.12989/was.2013.16.3.249, http://koreascience.or.kr/journal/view.jsp?kj=KJKHCF{&}py=2013{&}vnc=v16n3{&}sp=249, 2013.

Macagno, E.: Historico-critical review of dimensional analysis, Journal of the Franklin Institute, 292, 391–402, doi:10.1016/0016-0032(71)90160-8, 1971.

MacAyeal, D. R.: Large-scale ice flow over a viscous basal sediment: Theory and application to ice stream B, Antarctica, Journal of Geophysical Research, 94, 4071, doi:10.1029/JB094iB04p04071, 1989.

Mengel, M. and Levermann, a.: Ice plug prevents irreversible discharge from East Antarctica, Nature Climate Change, 4, 451–455, doi:10.1038/nclimate2226, http://www.nature.com/doifinder/10.1038/nclimate2226, 2014.

Morland, L. W.: Unconfined Ice-Shelf Flow, in: Dynamics of the West Antarctic Ice Sheet, edited by Van der Veen, C. and Oerlemans, J., pp. 99–116, Springer Netherlands, http://dx.doi.org/10.1007/978-94-009-3745-1{_}6, 1987.

Pattyn, F., Perichon, L., Durand, G., Favier, L., Gagliardini, O., Hindmarsh, R. C. a., Zwinger, T., Albrecht, T., Cornford, S., Docquier, D., Fürst, J. J., Goldberg, D., Gudmundsson, G. H., Humbert, A., Hütten, M., Huybrechts, P., Jouvet, G., Kleiner, T., Larour, E., Martin, D., Morlighem, M., Payne, A. J., Pollard, D., Rückamp, M., Rybak, O., Seroussi, H., Thoma, M., and Wilkens, N.: Grounding-line migration in plan-view marine ice-sheet models: Results of the ice2sea MISMIP3d intercomparison, Journal of Glaciology, 59, 410–422, doi:10.3189/2013JoG12J129, http://openurl.ingenta.com/content/xref?genre=article{&}issn=0022-1430{&}volume=59{&}issue=215{&}spage=410, 2013.

Pollard, D. and DeConto, R. M.: Modelling West Antarctic ice sheet growth and collapse through the past five million years, Nature, 458, 329–332, doi:10.1038/nature07809, http://www.nature.com/doifinder/10.1038/nature07809, 2009.

Pollard, D. and DeConto, R. M.: Description of a hybrid ice sheet-shelf model, and application to Antarctica, Geosci. Model Dev., 5, 1273–1295, doi:10.5194/gmd-5-1273-2012, http://www.geosci-model-dev.net/5/1273/2012/gmd-5-1273-2012.pdf, 2012.

Pollard, D., Deconto, R. M., and Alley, R. B.: Potential Antarctic Ice Sheet retreat driven by hydrofracturing and ice cliff failure, Earth and Planetary Science Letters, 412, 112–121, doi:10.1016/j.epsl.2014.12.035, http://dx.doi.org/10.1016/j.epsl.2014.12.035, 2015.

Rayleigh: The Principle of Similitude, Nature, 96, 396–397, doi:10.1038/096396d0, http://www.nature.com/doifinder/10.1038/096396d0, 1915.

Reynolds, O.: An Experimental Investigation of the Circumstances Which Determine Whether the Motion of Water Shall Be Direct or Sinuous, and of the Law of Resistance in Parallel Channels, Philosophical Transactions of the Royal Society of London, 174, 935–982, doi:10.1098/rstl.1883.0029, 1883.

Rignot, E., Mouginot, J., Morlighem, M., Seroussi, H., and Scheuchl, B.: Widespread, rapid grounding line retreat of Pine Island, Thwaites, Smith, and Kohler glaciers, West Antarctica, from 1992 to 2011, Geophysical Research Letters, 41, 3502–3509, doi:10.1002/2014GL060140, http://onlinelibrary.wiley.com/doi/10.1002/2014GL060140/full, 2014.

Sato, T. and Greve, R.: Sensitivity experiments for the Antarctic ice sheet with varied sub-ice-shelf melting rates, Annals of Glaciology, 53, 221–228, doi:10.3189/2012AoG60A042, http://www.igsoc.org/annals/53/60/t60A042.html, 2012.

Schoof, C.: Marine ice-sheet dynamics. Part 1. The case of rapid sliding, Journal of Fluid Mechanics, 573, 27, doi:10.1017/S0022112006003570, http://journals.cambridge.org/abstract{_}S0022112006003570, 2007a.

Schoof, C.: Ice sheet grounding line dynamics: Steady states, stability, and hysteresis, Journal of Geophysical Research,

112, F03S28, doi:10.1029/2006JF000664, http://doi.wiley.com/10.1029/2006JF000664, 2007b.

Schoof, C. and Hindmarsh, R. C. A.: Thin-Film Flows with Wall Slip: An Asymptotic Analysis of Higher Order Glacier Flow Models, The Quarterly Journal of Mechanics and Applied Mathematics, 63, 73–114, doi:10.1093/qjmam/hbp025, http://qjmam.oxfordjournals.org/cgi/doi/10.1093/qjmam/hbp025, 2010.

Scruton, C.: Wind tunnels and flow visualization, Nature, 189, 108–110, 1961.

Stahl, W. R.: Similarity and dimensional methods in biology., Science (New York, N.Y.), 137, 205–212, doi:10.1115/1.3640458, 1962.

Szücs, E.: Similitude and Modeling, Elsevevier Scientific Publishing Group, Amsterdam, 1980.

Thoma, M., Determann, J., Grosfeld, K., Goeller, S., and Hellmer, H. H.: Future sea-level rise due to projected ocean warming beneath the Filchner Ronne Ice Shelf: A coupled model study, Earth and Planetary Science Letters, 431, 217–224, doi:10.1016/j.epsl.2015.09.013, http://linkinghub.elsevier.com/retrieve/pii/S0012821X15005804, 2015.

Tsai, V. C., Stewart, A. L., and Thompson, A. F.: Marine ice-sheet profiles and stability under Coulomb basal conditions, Journal of Glaciology, 61, 205–215, doi:10.3189/2015JoG14J221, http://www.igsoc.org/journal/61/226/t14j221.html, 2015.

Tulaczyk, S., Kamb, W. B., and Engelhardt, H. F.: Basal mechanics of Ice Stream B, west Antarctica: 1. Till mechanics, Journal of Geophysical Research, 105, 463, doi:10.1029/1999JB900329, 2000.

Vialov, S. S.: Regularities of glacial sheilds movement and the theory of plastic viscours flow, Physics of the movements of ice IAHS, 47, 266–275, 1958.

Weertman, J.: Stability of the junction of an ice sheet and an ice shelf, Journal of Glaciology, 13, 3–11, http://adsabs.harvard.edu/abs/1974JGlac..13....3W, 1974.

Table 1. Parameter values as prescribed in the unscaled reference simulations for the flow-line setup (2D) and the three-dimensional channel setup (3D), respectively. For the scaling experiments the bed geometry (b_x and b_y) and the parameters a, A and C are multiplied with the scaling ratios from to Table 2. The terms "BC-300" and "BC0" refer to the bed geometries described in Feldmann and Levermann (2015a) and $b_{y,G}$ refers to y-component of the bed topography used in Gudmundsson et al. (2012).

Parameter	$2D_{ref}$	$3D_{ref}$	Unit	Physical meaning
a	0.6	0.5	$\mathrm{m\,yr^{-1}}$	Surface mass balance
b_x	"BC-300"	"BC0" - 300 m		x-component of bed topography
b_y	-	$b_{y,G}$		y-component of bed topography
A		10^{-25}	$\mathrm{Pa^{-3}s^{-1}}$	Ice softness
C		10^7	$\mathrm{Pa\,m^{-1/3}s^{1/3}}$	Basal friction parameter
g		9.81	$\mathrm{m\,s^{-2}}$	Gravitational acceleration
m		$1/3$		Basal friction exponent
n		3		Exponent in Glen's law
ρ_i		900	$\mathrm{kg\,m^{-3}}$	Ice density
ρ_w		1000	$\mathrm{kg\,m^{-3}}$	Sea-water density

Table 2. Scaling ratios as used for our numerical simulations. Prescribed scaling ratios are highlighted in blue, the other result from Eqs. (11)-(17), (29) and (30). Each row corresponds to a scaling experiment, that is carried out in flow line ("2D") and in a three-dimensional channel setup ("3D"). The parameters values prescribed in the simulations are obtained by multiplying b_x, b_y, C, a and A (see Table 1) with the given ratios α, β, γ, δ and ζ. The analytic values for $\dot{\chi}$ are used to fit the sections of linear grounding-line retreat in Figs. 5 and 6.

Simulation name	α	β	γ	δ	ζ	τ	$\dot{\chi}$
2D/3D~~REF~~ ref	1	1	1	1	1	1	1
$2D/3D_{\alpha=1,\beta=\frac{1}{2},\gamma=1}$	1	$\frac{1}{2}$	1	$\frac{1}{128}$	$\frac{1}{8}$	64	$\frac{1}{64}$
$2D/3D_{\alpha=\frac{1}{2},\beta=\frac{1}{2},\gamma=1}$	$\frac{1}{2}$	$\frac{1}{2}$	1	$\frac{1}{8}$	2	4	$\frac{1}{8}$
$2D/3D_{\alpha=\frac{1}{2},\beta=1,\gamma=1}$	$\frac{1}{2}$	1	1	16	16	$\frac{1}{16}$	8
$2D/3D_{\alpha=1,\beta=\frac{1}{2},\delta=1}$	1	$\frac{1}{2}$	$(\frac{1}{2})^{7/3}$	1	16	$\frac{1}{2}$	2
$2D/3D_{\alpha=\frac{1}{2},\beta=\frac{1}{2},\delta=1}$	$\frac{1}{2}$	$\frac{1}{2}$	$\frac{1}{2}$	1	16	$\frac{1}{2}$	1
$2D/3D_{\alpha=\frac{1}{2},\beta=1,\delta=1}$	$\frac{1}{2}$	1	$(\frac{1}{2})^{-4/3}$	1	1	1	$\frac{1}{2}$

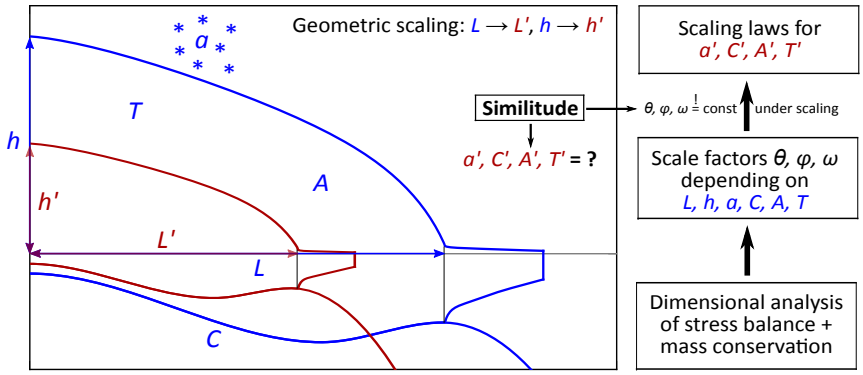

Figure 1. Schematic of the similitude-analysis method carried out in this study. A reference system (blue ice sheet and bed topography) with geometric scales h and L, time scale T and physical parameters ice softness A, basal friction coefficient C and surface mass balance a is scaled in horizontal and vertical direction (red contours, primed system). The goal is to derive the scaled parameters of the primed system under which dynamic similarity between both ice sheets holds. A dimensional analysis of the governing equations yields dimensionless scale factors which have to remain ~~constant~~ the same under scaling to attain similitude. The resulting scaling laws determine the scaled (primed) parameters.

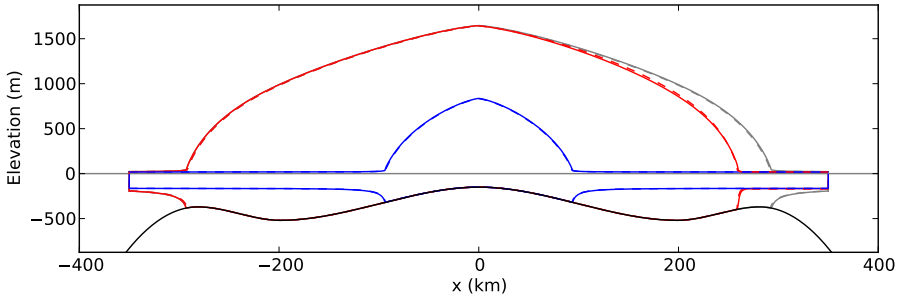

Figure 2. Ice sheet profiles at three different stages of the flow-line simulations $2D_{\alpha=\frac{1}{2},\beta=\frac{1}{2},\gamma=1}$ (continuous) and $2D_{\text{ref}}$ (dashed). Output of the reference simulation is scaled by factor 0.5 in both horizontal and vertical direction to allow for comparison of shapes between the two simulations.

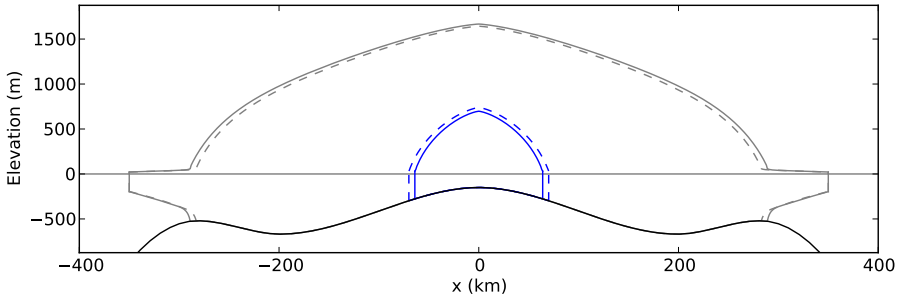

Figure 3. Steady-state ice-sheet profiles for cross section along the centerline ($y = 0$) of the three-dimensional channel setup for simulations $3D_{\alpha=\frac{1}{2},\beta=\frac{1}{2},\gamma=1}$ (continuous) and $3D_{\text{ref}}$ (dashed). Output of the reference simulation is scaled by 0.5 in both horizontal and vertical direction to allow for comparison of shapes between the two simulations.

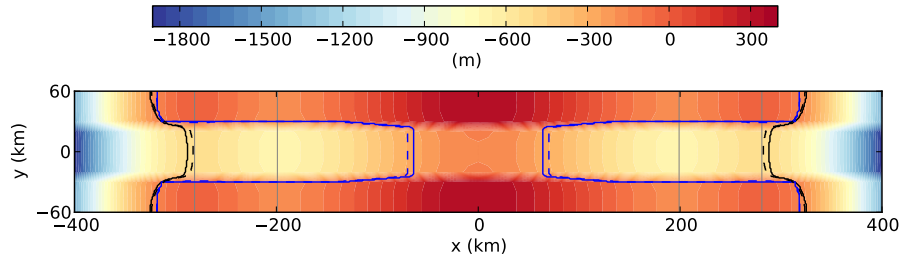

Figure 4. Bed topography of the three-dimensional channel setup, here shown in the scaled version with $\alpha = \beta = 0.5$ (see Fig. 3 for a cross section along $y = 0$). Steady-state grounding-line positions for simulations $3D_{\alpha=\frac{1}{2},\beta=\frac{1}{2},\gamma=1}$ (continuous) and $3D_{\text{ref}}$ (dashed). Grey lines mark the position of the coastal sill and the bed depression, respectively. Output of the reference simulation is scaled by 0.5 in horizontal direction to allow for comparison of shapes between the two simulations.

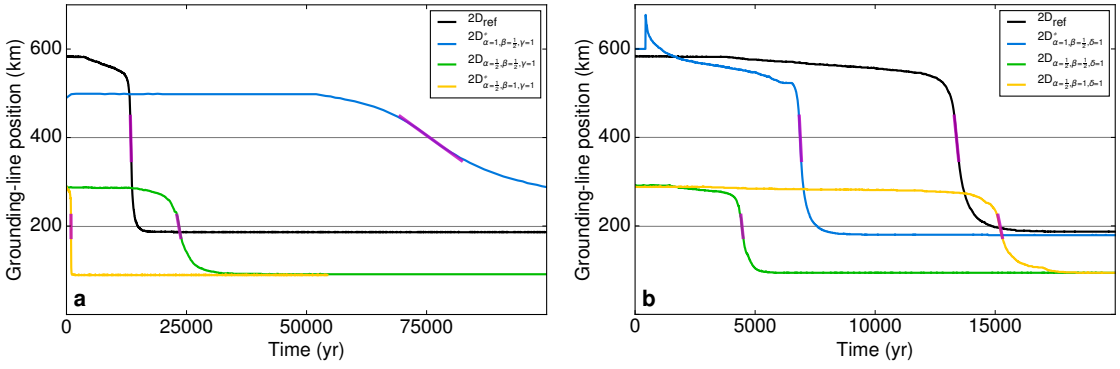

Figure 5. Time series of grounding-line position for the reference and three geometrically scaled flow-line experiments ~~for which~~ with **(a)** identical basal friction and **(b)** identical surface mass balance~~is held constant~~, respectively. Grey horizontal lines indicate location of the minimum of the bed depression for both the scaled und unscaled case around which the grounding line retreats unstable and retreat rates are approximately constant. In ~~this~~ the range of ± 50 km around the minimum depression the slope of the curve of the unscaled simulation is fitted to obtain a reference retreat rate of ~~0.47~~ 0.54 km/yr (purple slope fitted to black curve)~~which~~. This slope is used to predict the slopes, i.e., retreat rates, for the scaled experiments (other curves ~~overlayn~~ overlaid by purple lines with predicted slopes) according to Table 1.

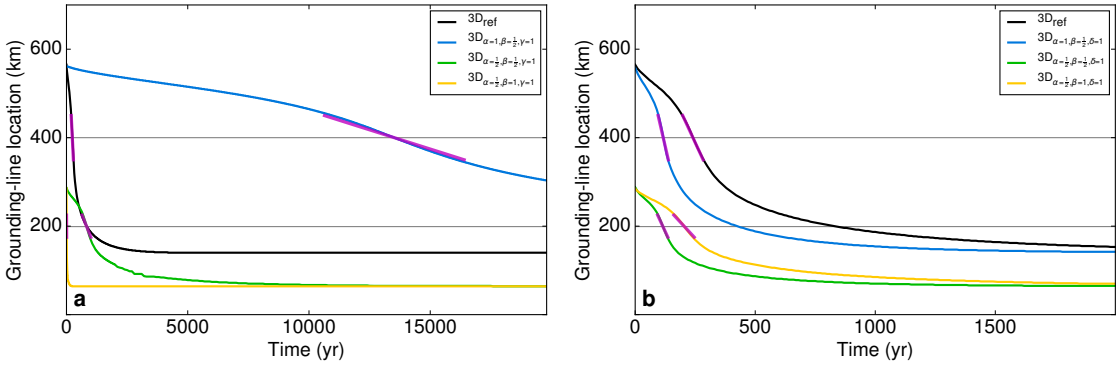

Figure 6. Time series of centerline grounding-line position (along $y = 0$) for the reference and three geometrically scaled 3D channel experiments ~~for which~~ with **(a)** identical basal friction and **(b)** identical surface mass balance~~is held constant~~, respectively. The ~~Fitting~~ fitting method is the same as described in Fig. 5 with a reference retreat rate of 1.18 km/yr.

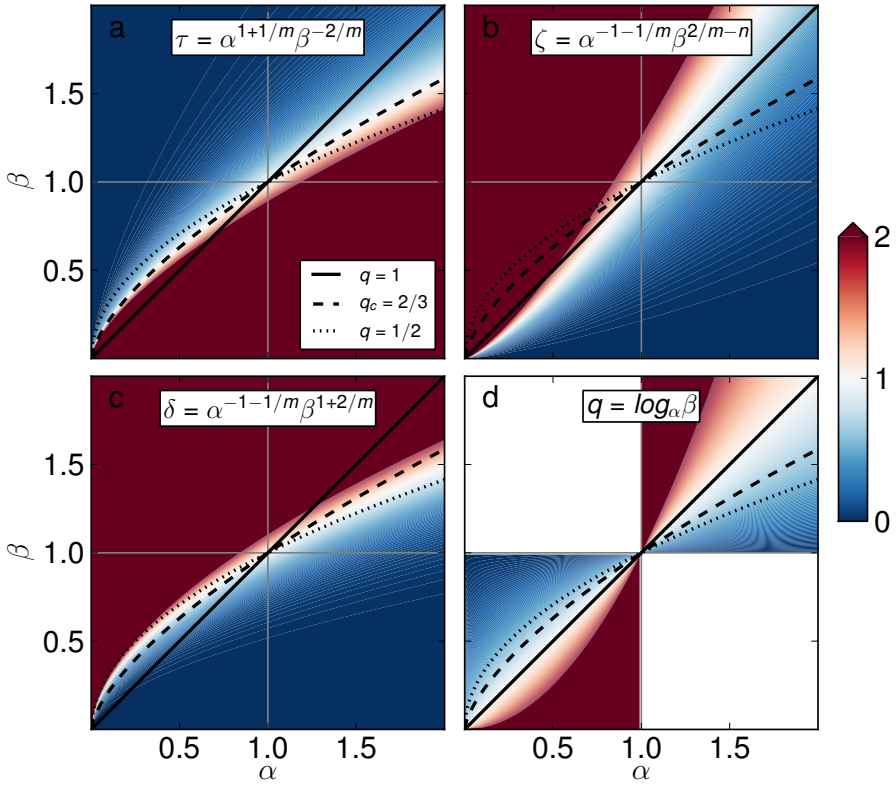

Figure 7. Scaling of **(a)** response time (Eq. 11), **(b)** ice softness (Eq. 16) and **(c)** surface mass balance (Eq. 15) in the α-β phase space for $\gamma = 1$ and $m = 1/3$. Panel **(d)** shows value of the exponent q if the two horizontal scales are linked according to Eq. (32). Dotted line represents scaling of an ice sheet with Vialov proportions. Dashed line denotes critical threshold $\tau = 1$.

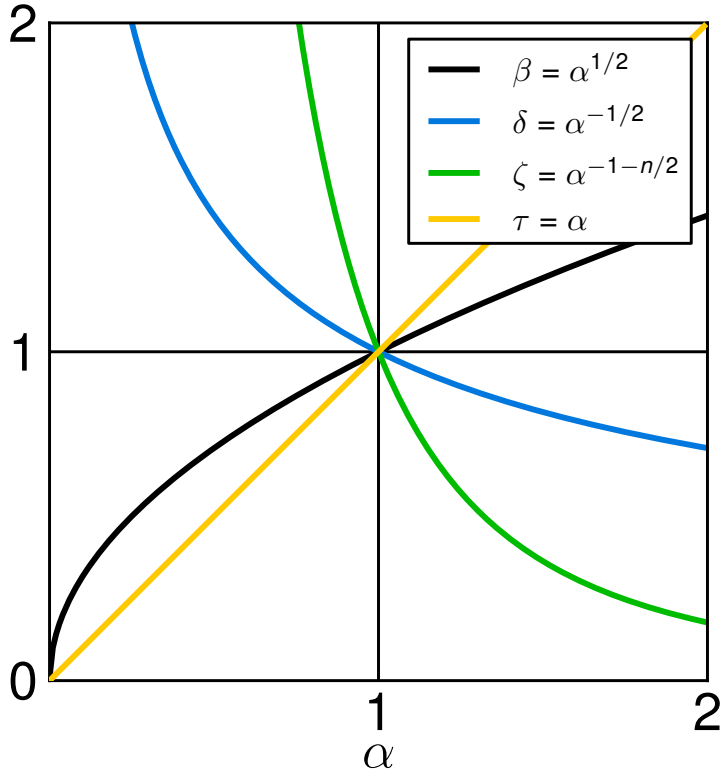

Figure 8. Scaling of response time τ, surface mass balance δ and ice softness ζ under the assumption of Vialov-type geometric scaling ($\beta = \alpha^{1/2}$) and ~~constant~~ identical basal friction ($\gamma = 1$). The resulting scaling conditions are independent of m and given in the legend (n=3).

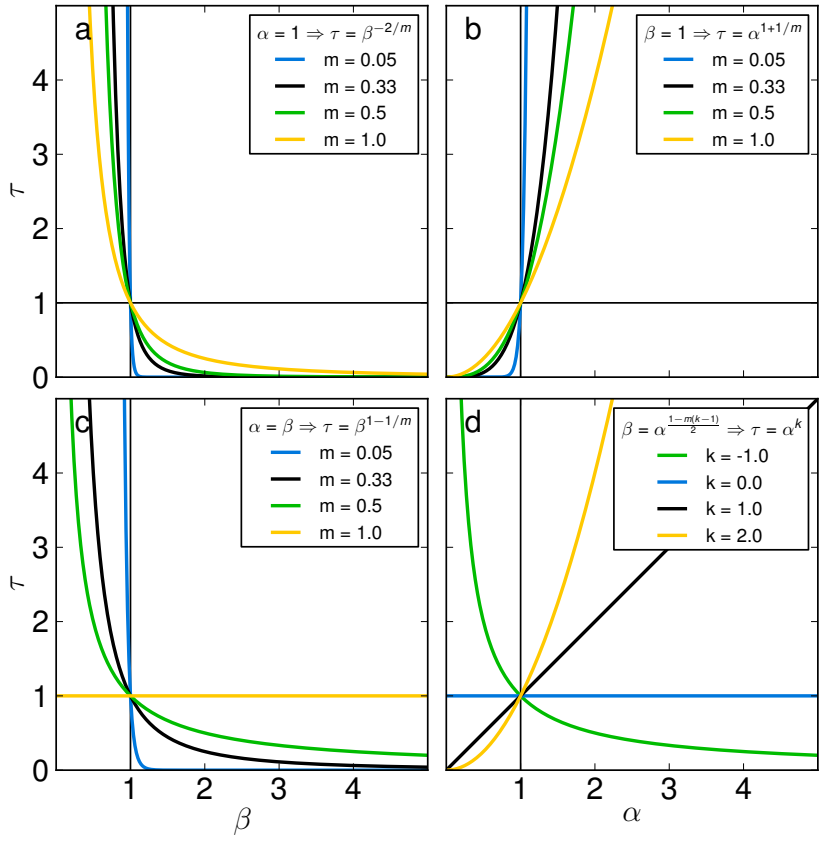

Figure 9. Response-time scaling for hypersurfaces through the α-β-m phase space according to Eq. (31) for **(a)** $\alpha = 1$, **(b)** $\beta = 1$, **(c)** $\alpha = \beta$ and **(d)** the constraint that the response time scales independently of m. In each panel the legend gives the scaling law for τ that results from the applied constraint.

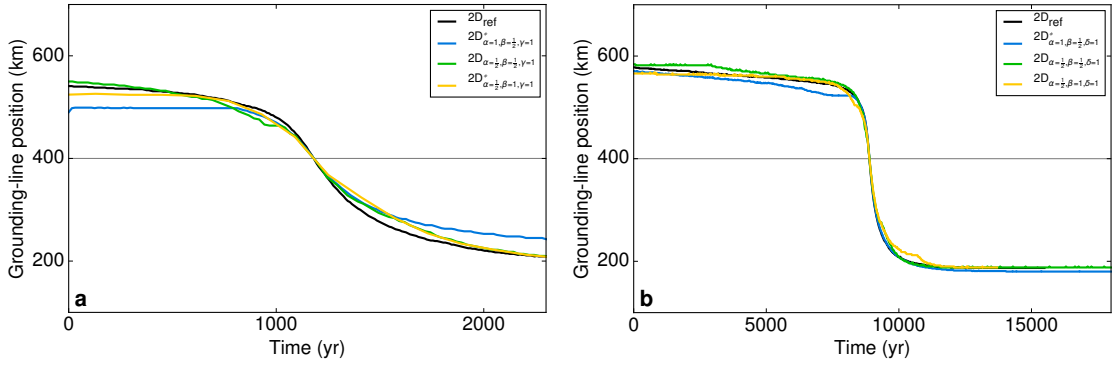

Figure C1. Scaled time series of grounding-line position for the reference and three geometrically scaled flow-line experiments with **(a)** identical basal friction and **(b)** identical surface mass balance, respectively. For better comparison the grounding-line curves are shifted along the time axis to overlap where the grounding line passes the minimum of the bed depression (grey horizontal line). Around this point the scaled curves of unstable grounding-line retreat approximately collapse into a single curve, indicating that the scaled speed of the grounding-line instability is approximately the same throughout the ensemble of scaling experiments. See Fig. 5 for unscaled version of this figure.

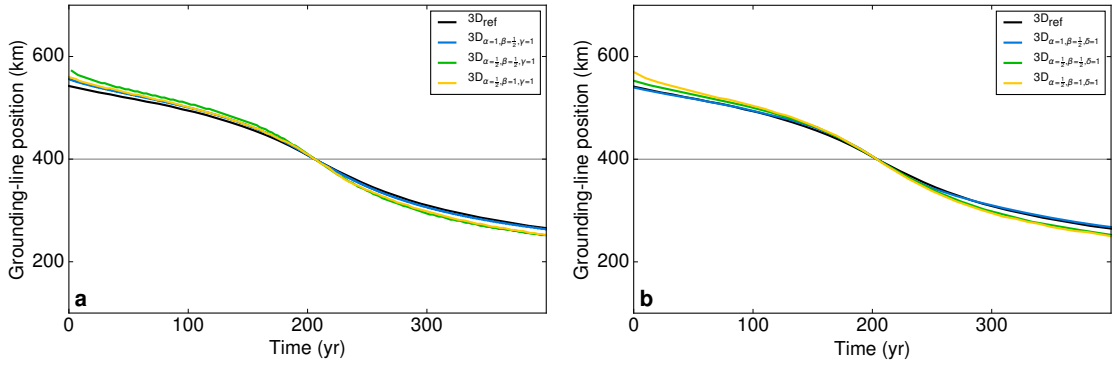

Figure C2. Scaled time series of centerline grounding-line position (along $y = 0$) for the reference and three geometrically scaled 3D channel experiments with **(a)** identical basal friction and **(b)** identical surface mass balance, respectively (analogous to Fig. C1). See Fig. 6 for unscaled version of this figure.